# POLYMER/CERAMIC HYBRID SEPARATORS FOR LITHIUM-SULFUR BATTERIES

A Thesis

Presented to the Faculty of the Graduate School

of Cornell University

In Partial Fulfillment of the Requirements for the Degree of

Master of Science

by

Travis Matthew O'Neil

August 2019

# ABSTRACT

Lithium-sulfur (Li-S) is a promising candidate for next-generation batteries. There has been much effort in researching novel Li-S cathode materials to overcome inherent drawbacks, but limited attention to separator improvements, which can drastically affect ion diffusion and overall battery safety aspects.

In this work, gas-assisted electrospinning is used to develop polymer/ceramic non-woven separators with polyimide (PI) and a polysilsesquioxane (PSSQ) ceramic. These separators are thermally stable well above temperatures seen in typical battery abuse conditions and retain their structural integrity even after being ignited. In Li-S cells, superior cycling performance is seen at high charge/discharge rates, owing to high ionic conductivity through the fibrous structure and favorable electrolyte interactions with PSSQ.

To extend the previous work, a graphene interlayer was coated onto PI/PSSQ with an air-controlled electrospray method. This interlayer served as a physical barrier to hinder polysulfide shuttling and a “secondary cathode” to further improve battery rate capability performance.

# BIOGRAPHICAL SKETCH

Travis O'Neil was born in Johnson City, New York on September 14th, 1995, and was raised in the nearby small town of Maine, NY. After graduating from Maine-Endwell High School in 2013, he decided to pursue Chemical Engineering at Clarkson University in the fall of that same year. This put him in the best position to follow his dream for developing next-generation renewable energy technologies. He was fortunate enough to obtain internships each summer between his four years there, allowing him to put what was learned in the classroom to the test while developing his passion for research. He completed a Research Experience for Undergraduates (REU) internship in the summer of 2015 at The Pennsylvania State University, as part of the National Nanotechnology Infrastructure Network (NNIN). Performing research in a state-of-the-art nanofabrication clean room facility there opened him up to the world of academic research. His 2016 summer internship as the R&D Elastomers intern at Momentive Performance Materials in Waterford, NY taught him about the pace of research in a global company. From these experiences, he knew that research in an industrial setting was the ideal career path. After graduating from Clarkson University in May of 2017 with a Bachelor of Science in Chemical Engineering, he decided to pursue a Master of Science in Chemical Engineering at Cornell University. Since then, he has been working under the supervision of Dr. Yong Lak Joo, developing polymer/ceramic hybrid non-woven separators for next-generation lithium-sulfur batteries.

To mom, dad, Tyler, and April

ACKNOWLEDGMENTS

I would like to express my sincerest gratitude to my research advisor, Dr. Yong Lak Joo, for all his help and guidance over these past two years. What I have learned from you will prove invaluable over the course of my career, wherever it takes me. I am also thankful to Dr. Margaret Frey, who served on my special committee. A special thanks goes out to Dr. Kathleen Vaeth and Dr. Tobias Hanrath, who graciously hired me to be a Teaching Assistant for the newly revamped Product Design course in my first year, and then asked me to help again the next year. I was able to develop and refine numerous communication and teaching skills working with you both.

I acknowledge and appreciate all the support from my friends at Cornell, who made enjoy my two years here even when the going got tough. In particular I would like to thank Dr. Jin Hong Lee, Rui, and Willy for getting me started on lithium-sulfur, George and Somayeh for your help along the way, and Chris, Mounica, Shubham, Andrew, Ghazal, Joe, Mohammed, Yash, Leyan, Chao-Wen, Snatika, Jasper, and all other Joo Group members for making the offices/labs enjoyable spaces to work in.

Finally, I would not be where I am today without my Mom and Dad, Tyler, Charlie, and April. Your endless love and support mean more to me than I can put into words.

TABLE OF CONTENTS

LIST OF FIGURES

LIST OF TABLES

# Chapter 1. Introduction

## 1.1 Battery Overview

### 1.1.1 The Need for Improved Energy Storage

Modern living and a more interconnected world have caused the global demand for energy to continuously rise. It is projected that the total energy consumption will increase to 240,000 TWh by year 2040, up from 154,000 TWh in year 2010 and just 58,000 TWh in year 1971.[1,2] This exponentially increasing demand has required an increased electricity generation capacity. Historically, energy has been generated using fossil fuel sources, such as coal or gas-powered plants. These were logical choices because fossil fuels are abundant and cheap, with well-understood and relatively simple processes to do work with the stored energy.[3] In the year 2013, approximately 67% of electricity generation worldwide was produced with fossil-fuel based sources.[4]

In the past few decades, there has been a growing concern over the greenhouse gases emitted in the process of generating energy with fossil fuels. Carbon dioxide, methane, and nitrous oxide concentrations in the atmosphere have drastically increased since the industrial revolution. This has correlated with an increasing global temperature, a phenomenon known as global warming. Renewable energy technologies such as wind turbines and photovoltaics are part of the solution to this issue, but they face some fundamental challenges. The main issue with technologies such as these is that they are intermittent by nature; wind or sunlight are not always available to generate power. Therefore, they won't be able to meet full energy demand on their own. It is energy storage that will allow intermittent renewable energy sources

to realize their full potential by storing excess electricity generated at peak operating hours.

Improved energy storage is also needed for consumer electronics and electric vehicles (EVs). Consumer demand and technological advances are straining state-of-the-art battery technology, pushing it to the limits. Longer battery life, higher capacity, faster charging, and improved safety have been the main necessities to keep pace with the evolution of technology.[5] The push for higher market penetration of EVs in recent years has brought these issues to the forefront. Battery pack costs have typically made EVs significantly more expensive than their ICE vehicle counterparts, but these costs have been steadily declining in recent years.[6] Battery pack costs are projected to be less than 150 USD/kWh by the year 2025 in some estimates, which will help make EVs more affordable to the average consumer.[7] Much research has gone into overcoming the technological challenges associated with batteries, as will be discussed later. First, the principles electrochemical energy storage with batteries will be detailed.

### 1.1.2 Battery Basics

The concept of a battery first materialized when in the 1800, Alessandro Volta constructed his famous "pile".[8] A typical battery can be broken down into four main parts: the cathode, anode, electrolyte, and separator. The cathode and anode are the electrodes at which stored chemical energy is converted into useful electrical energy. During a discharge process, the anode undergoes an oxidation reaction to generate ions and release electrons into an external circuit, where they can perform useful work

such as powering a device. The ions combine with electrons at the cathode to complete the circuit, known as a reduction reaction. Electrolyte allows this diffusion of ions from one electrode to the other, so that the redox reactions can occur.[9] Typically, battery electrolyte consists of a salt dissolved in a solvent, allowing for ion transfer. The separator provides an electrically insulating barrier between the two electrodes, preventing them from contacting and short-circuiting the battery. It must allow ions to diffuse from one electrode to the other at sufficient rates such that the overall performance is not limited by ion transport. Although it is not directly involved with the chemical reactions, the separator is a critical component for batteries, and is the focus of this research.

### 1.1.3 Types of Batteries

Over the years various battery chemistries and configurations have been investigated, each with their own benefits and deficiencies. The first rechargeable (secondary) battery was based on a lead-acid chemistry invented by Plantè in 1859, which is a system still used today.[10] The cell consists of a lead(IV) oxide cathode and an elemental lead anode, with a concentrated sulfuric acid electrolyte.[11] It has been widely used for automobile and renewable energy storage applications but suffers from low specific energy (about 30-40 Wh/kg) and energy density.[12] These drawbacks have largely prevented their use in consumer electronics and smaller devices.

The next significant development in secondary batteries was in 1899 when Jungner developed the nickel-cadmium (Ni-Cd) battery, which utilizes a cadmium anode and nickel cathode.[13,14] This chemistry provided a more energy dense (50-60 Wh/kg)

option over lead-acid chemistries, allowing it to penetrate diverse markets such as personal and commercial electronics, communications, and many other portable applications, and reached a market of was $3 billion in 1995.[15] However, concerns over cadmium toxicity stalled their use. Ni-Cd battery usage has largely been banned in China and the EU over concerns of environmental damage due to improper battery disposal and recycling, paving the way for other battery chemistries to take over the market.[16–18]

Nickel metal hydride (NiMH) batteries were heavily researched starting in the 1970's, but initially suffered from unstable metal hydride electrodes.[19] They are similar to Ni-Cd in terms of operating voltage and cycling performance, while eliminating toxic cadmium and achieving a high specific energy.[20,21] They work by storing hydrogen in the form of a solid-state metal hydride anode and releasing it in an electrochemical reaction during the discharge, while nickel hydroxide serves as the cathode. These batteries were first commercialized in 1989 and have a large share of the battery market today due to their long service life and robustness in a range of operational conditions and temperatures.[22,23] They have been used for both stationary and portable applications, most notably in plug-in hybrid and electric vehicles. Typically they suffer from poor cycle life and high costs, but recent advances have overcome these challenges at the individual cell level.[24] A specific energy of 140 Wh/kg has also been achieved, making it more comparable with current lithium-ion chemistries for electric vehicle applications.[25]

Lithium-based batteries have received a lot of attention over the past few decades due to lithium having the highest specific capacity (3,860 mAh/g) and lowest

electrochemical potential (-3.04 V vs. standard hydrogen electrode) of all metals.[26,27] The first rechargeable Li battery was developed by Whittingham at Exxon in the 1970's,[28] but it used pure lithium metal as an electrode, which comes with various challenges. During the plating/stripping of Li metal while cycling the battery, lithium ions unevenly deposit onto the surface of the electrode, forming what are known as dendrites.[29,30] These dendrites eventually grow enough to pierce the separator and short circuit the cell, which is the main cause of safety hazards associated with Li anodes. Also, Li anodes suffer from low Coulombic efficiency, leading to fast capacity fading. The arrival of Li-ion batteries that avoid the problems associated with using metallic lithium diverted research focus from pure lithium metal chemistries.

Li-ion batteries operate through two intercalation electrodes, where the lithium ions insert themselves into the structure of the electrodes without causing significant structural change.[10] Fig. 1.1 compares energy densities for different battery chemistries, showing why Li-ion has been dominant in the battery market over those previously mentioned.[31] The first major breakthrough in Li-ion batteries came when Goodenough introduced the lithium cobalt oxide ($Li_xCoO_2$) cathode in 1980,[32] offering a higher operating voltage than the $Li_xTiS_2$ intercalation predecessor and overcoming many of its challenges.[33] Sony commercialized this $Li_xCoO_2$ cathode with a graphite anode in 1990, and Li-ion chemistries have since revolutionized many industries.[33–35] Many other intercalation cathode materials have since been proposed, with various tradeoffs in terms of energy density, specific capacity, stability, and cost.[36] The graphite anode has largely remained unchanged commercially since the Li-ion debut by Sony. Significant research effort has been devoted to incorporating

silicon into the anode since it has a very high theoretical specific capacity of 4,200 mAh/g, but suffers from 420% volume expansion during lithiation de-lithiation reactions, hindering its success.[36–38] Modern technological demands are pushing lithium-ion batteries to their practical limits, requiring higher energy density and power output. Li-metal based battery chemistries will enable next generation technologies by providing the necessary energy storage capabilities, but their challenges must be overcome.

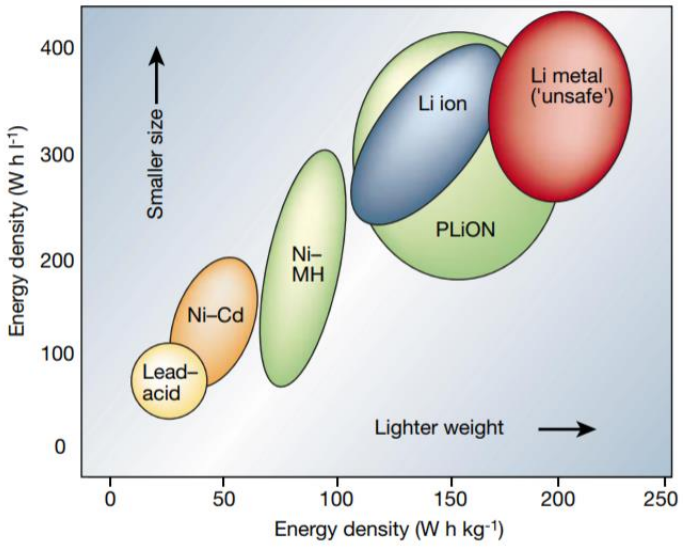


**Figure 1.1** Volumetric vs. gravimetric energy density for different battery chemistries.[31]

Various next-generation Li-metal based chemistries being researched globally. Lithium-air batteries have received much attention recently for potential EV applications due to their high theoretical specific energy density (5,200 Wh/kg) approaching that of the gasoline used in internal combustion engine vehicles (13,000

Wh/kg theoretical, 1,700 Wh/kg practical).[39] However, the cathode material in the chemistry is gaseous oxygen, so a three-phase solid-liquid-gas heterogeneous reaction needs to occur for the battery to discharge, and for elemental oxygen to be reduced to lithium oxides. Some of the major issues are the poor reversibility of the discharge product,[40,41] clogging of reaction sites on the porous conductive cathode support,[42,43] and electrolyte decomposition.[44–46] Due to these limitations, lithium-air research is still in its infancy. Lithium-sulfur (Li-S) batteries have also been very promising, with a theoretical energy density of 2,600 Wh/kg.[47] This battery chemistry is currently more developed than Li-air and is the focus of this work. Therefore, it will be discussed more thoroughly in the following section.

### 1.1.4 Lithium-Sulfur (Li-S) Batteries

Lithium-sulfur batteries have been heavily researched in the past few decades, gaining more traction as more industries are looking beyond Li-ion for next generation technology applications. Sulfur is abundant in the Earth's crust and one of the major byproducts of refining oil, and is therefore relatively cheap compared to the rare-Earth metals used in Li-ion cathodes.[48] Sulfur is also nontoxic and environmentally benign, making it attractive compared to the cobalt used in Li-ion.[49,50] Unlike Li-ion batteries, which operate through intercalation and de-intercalation reactions, Li-S operates through a cascade of reactions, where elemental sulfur ($S_8$) is eventually reduced to $Li_2S$ through a series of lithium polysulfide ($Li_2S_X$, where $1 \leq X \leq 8$) intermediates.[51] This series of reactions is what gives the Li-S chemistry its high theoretical specific capacity (1,675 mAh/g) compared to that of the Li-ion electrodes, making it a very

promising electrochemical storage material.[52] There are a few challenges associated with sulfur that limit its practical use in commercial applications.

The first is that elemental sulfur, $S_8$, and the final discharge product, $Li_2S$, are insulating compounds. Due to this, a significant fraction of the cathode by mass consists of conductive materials, such as carbons, to ensure proper electrical contact.[52,53] This high percentage of inactive carbons drastically reduces the practical energy density of Li-S batteries. Capacity fading results when the insoluble $S_8$ and $Li_2S_2$/$Li_2S$ species clog up the porous carbons in the cathode, preventing lithium ion diffusion into the pore, or are otherwise not in contact with an electronically conductive surface.[52,54] This issue is pronounced when higher sulfur loading is used, leading to poor active material utilization.

The second challenge is associated with the various polysulfides formed that give this chemistry its high theoretical capacity. The higher order polysulfides ($Li_2S_X$, $3 \leq X \leq 8$) are soluble in the typical organic electrolytes used and tend to diffuse to the lithium metal anode during discharge.[55,56] This phenomenon is known as "polysulfide shuttling" and is one of the major challenges facing Li-S. Polysulfide shuttling results in capacity fade during cycling and low Coulombic efficiencies as the soluble polysulfide species are further reduced at the lithium anode to form lower-order polysulfides, which can then diffuse back to the cathode to be oxidized to higher-order ones.[56,57] If the polysulfides are reduced to $Li_2S_2$ or $Li_2S$ at the anode, then insoluble deposits are formed on the lithium surface and that active material is lost.

A third challenge is the 80% volume expansion of the active materials as the elemental $S_8$ is reduced to $Li_2S$ and vice-versa, which is still much less than 420%

change of Si in next-generation Li-ion anodes.[53] This volume change can destroy the cathode structure through mechanical cracking, leading to lost electrical contact with the insulating species. Volume expansion has largely been mitigated by using porous carbon materials, as will be discussed next.

Numerous approaches have been taken to address these issues. Lithium nitrate ($LiNO_3$) has been shown to be an effective electrolyte additive to help protect the lithium anode from polysulfide reactions during cycling.[58] It functions by depositing an ionically conductive layer onto the lithium anode surface, allowing $Li^+$ but not polysulfides to diffuse through.[59] $LiNO_3$ is continuously consumed during cycling to passivate newly exposed lithium, so higher concentrations of $LiNO_3$ in the electrolyte have also shown some promise prolonging cycle life.[60]

Some of the most well-studied are the use of sulfur-impregnated porous carbons or sulfur chemisorption to ensure proper electrical contact with the insulating species through high surface area and provide a framework to help prevent the migration of the soluble polysulfide species.[53,61] The use of lightweight carbons helps to minimize the loss of gravimetric energy density through the added cathode mass. Various carbons have been investigated, such as carbon nanotubes (CNTs),[62–64] micro/mesoporous carbon particles,[61,65,66] carbon nanofibers (CNFs),[67–69] and reduced graphene oxide (rGO).[70–72] These methods have been effective, to various degrees, at improving electrical contact with the insulating active material and trapping polysulfides in the cathode region, thus improving overall capacity and cycle life.

Another approach to mitigate polysulfide shuttling is through the addition of an interlayer, which is an extra barrier between the sulfur cathode and separator. Several

types of interlayers have been employed, helping to block the shuttling intermediates through means such as physical blocking, chemisorption, ionic shielding, or any combination of the three.[73–75] Interlayers have been shown to reduce capacity fade by trapping the soluble polysulfides and largely preventing them from reaching the anode. Using a conductive interlayer, through added carbons[76–78] or ion-conductive polymers,[79–81] has the added benefit of reactivating any polysulfides trapped in the interlayer by providing an electrically conducting pathway, thus also improving the capacity compared to cells cycled without the added barrier.

In general, much lithium sulfur research has been dedicated to solving the issues inherent in the chemistry at the cathode, with limited effort towards improved or novel separators. Similar improvements for the separator as needed in Li-ion chemistries will be needed for Li-S. However, the electrochemical mechanisms present in Li-S cells introduce unique challenges for separator materials, which novel designs can help to overcome.

## 1.2 Separator Overview

The separator is a critical component of an electrochemical cell, providing an insulating barrier between the electrodes. Although it doesn't directly participate in the electrochemical reactions, it is important in controlling the rate of ion diffusion from one electrode to the other while acting as the electrolyte reservoir. An ideal separator would be as thin as possible to minimize the resistance to ion diffusion. In practice, however, too thin of a separator degrades its mechanical robustness, increasing the risk of cell failure through short-circuiting if the electrodes contact each other after

separator damage.[82] The structure and properties of the separator drastically influence the overall performance of a battery cell.

### 1.2.1 Separator Requirements

In all battery chemistries, the separator should be electrochemically stable and chemically inert during operation. If the material degrades during cycling, then this could lead to poor cell performance or complete battery failure. Impurities introduced by the separator can lead to unwanted side reactions as well. The harsh chemicals and strong oxidizing/reducing environment within a battery cell limits the types of materials applicable for separator use.[83]

The separator must also be mechanically strong and robust. Sufficient tensile strength is necessary to withstand the winding process used in commercial battery fabrication. Also, the puncture strength of the separator should be high enough to prevent penetration by electrode active materials, which leads to a cell short-circuit.

Thermal stability is also one of the main concerns of separator materials.[84] If a battery is operated at elevated temperatures or under high abuse conditions, the separator should maintain its dimensional integrity. It is known that in lithium-ion chemistries, a series of exothermic side-reactions occur as low as 80 °C.[85] If the heat dissipation is lower than the heat generation, then this causes the battery temperature to rise even further, leading to a cascade of side reactions as the electrolyte and battery materials degrade further. Separator deformation under high temperatures leads to cell short-circuit and possible catastrophic failure (fires or even explosions), as this exacerbates the thermal runaway process. This is especially important in EV or

hybrid-EV applications, where the batteries may see elevated temperatures more regularly.[86]

Another main requirement is proper electrolyte wetting and uptake. The separator should be able to sufficiently absorb electrolyte to facilitate ion transport. Hydrophilic separator material is more easily wetted it is by the typical organic liquid electrolytes, which facilitates the battery assembly process. Higher electrolyte uptake lowers the overall resistance of the cell as it allows ions to more easily diffuse from one electrode to the other during cycling. Apart from the material hydrophobicity, electrolyte uptake is also strongly affected by the porosity and pore size of the membrane.

The separator pore size needs to be small enough to block electrode materials from diffusion from one to the other, or otherwise trapped and lost for further electrochemical reactions. A pore size under 1 μm has been designated as the target for lithium-ion batteries for this reason.[87] Highly tortuous and uniform pore structures can also limit the impact of dendrites, by allowing more uniform metal deposition and impeding their growth. Separator porosity influences how much electrolyte the membrane can hold overall, by controlling the available free space. Too low porosity can lead to insufficient electrolyte between the electrodes, limiting ion diffusion and increasing the overall resistance of the cell. Too high porosity can lead to low mechanical strength and physical deformation/shrinking after being soaked with electrolyte. Separator porosity can be measured by the equation:

$$Porosity\ (\%) = \frac{W - W_0}{\rho_L V_0} \times 100 \qquad (1)$$

where $W$ and $W_0$ are the weight of the separator before and after liquid immersion (typically n-butanol), $\rho_L$ is the density of the liquid, and $V_0$ is the geometric volume of the separator.

### 1.2.2 Types of Separators

Separators can be separated into several main categories: microporous membranes, modified microporous membranes, non-woven mats, and composite membranes. Each type of separator typically excels in one or more of the requirements listed above but falls short in some of the others. The main properties of each will be briefly discussed, as numerous separator reviews have nicely summarized major findings and processing methods.[82,87,88]

Microporous membranes are so named because they contain micrometer-sized pores. They are typically made of polyolefins such as polypropylene (PP), polyethylene (PE), or blended PP/PE, and have been the most commercialized type of separator for Li-ion battery applications due to their excellent mechanical strength, chemical stability, and relatively low cost. There are both dry and wet processing methods to manufacture these separators, with each changing the overall morphology and behavior of the resulting membrane.[83] The drawbacks of polyolefin microporous separators are that they suffer from low wettability from common polar organic liquid electrolytes due to their hydrophobic nature, and that they suffer from low porosity and thermal stability.[89] Celgard separators, typically microporous PP or layered PP/PE materials, are the most commonly used separator reference in literature.[83] Microporous membranes have been made with other polymers, such as polyacrylonitrile (PAN)[90,91]

and polyvinylidene fluoride (PVDF),[92] typically through phase-inversion or casting methods. These polymers help to overcome some of the limitations of using polyolefins.

Modified microporous membranes also help to overcome the limitations of polyolefin microporous membranes. These membranes undergo surface alterations to improve properties such as electrolyte wettability, electrolyte retention, and thermal stability. High-energy irradiation has been used to graft hydrophilic constituents onto the surface of microporous polyolefin membranes or just crosslink the polyolefins themselves.[93,94] Gamma ray irradiation was shown to increase the thermal stability and change the pore structure compared to non-treated PE membranes.[94] The irradiation crosslinked the surface PE polymer chains, leading to enhanced rate capability in a Li-ion cell. Electron beam and plasma irradiation have also been used to graft monomers such as acrylonitrile[95], glycidal methacrylate[93], and methyl methacrylate.[96] Another approach to modify microporous membranes has been to apply different polymeric coatings to improve the overall properties of the separator. Polymers such as poly(methyl methacrylate) (PMMA),[97] ethylcellulose,[98] cellulose aerogel,[99] and acrylonitrile-methyl methacrylate copolymers[100] have been applied to polyolefin separator surfaces, improving properties such as thermal stability, electrolyte wettability, and electrochemical performance. A unique coating of polydopamine was dip-coated onto the surface of PE separators, resulting in a more hydrophilic surface and decreased the electrolyte contact angle, enhanced ionic conductivity, and improved cycle life and high-rate cyclability.[101]

Non-woven mats are fibrous membranes characterized by significantly higher porosity compared to microporous separators. Fibers are bonded together by mechanical, physical, or chemical means to give these mats their mechanical integrity. Non-woven mats can be made from dry methods such as melt blowing, or wet processes such as papermaking methods, wet-laid process, or spinning methods.[87] A thermoplastic bonding that has a lower melting temperature than the base polymer can be used to bond the base polymer fibers together after high-temperature calendering.[102] The issue with most methods of producing non-woven fiber mats is that fibers and pore size are too large to be practically used in lithium-based batteries, without sacrificing energy density due to a larger separator being needed. With traditional Li-ion battery separators being in the 25-50 μm thickness range, large fiber diameters limit the number of fibers that can span such small thicknesses, leading to larger pores and a greater chance of short-circuit. Electrospinning has been introduced as a facile and scalable method for making non-woven mats with sub-micron fibers and is now the one of the main ways for making non-woven separators for battery applications.[103] It is the method used in this work and will therefore be discussed in more detail in the next section. Overall, the high porosity and interconnected pore structure of non-woven fiber mats provides greater electrolyte uptake than traditional microporous separators. This has been shown to improve ionic conductivity, leading to improved rate capability performance as the electrochemical reactions aren't limited by ion diffusion. Many different polymers have been investigated in non-woven battery separator applications, including PVDF, PAN, PMMA, polyimide (PI), and blends/copolymers.[87,102,104,105] The various polymers used have different crystallinity

and surface properties, impacting their behavior with electrolytes and lithium ions. The types of polymer chosen also significantly impact mechanical and thermal stability. Some drawbacks of non-woven separators include lower mechanical strength compared to microporous membranes due to their fibrous structure, and relatively slow fabrication times.[103]

Composite separators introduce inorganic material into the separator to impart their beneficial thermal, mechanical, and chemical properties. This typically involves coating inorganic particles onto the polymer surface or adding them directly into the polymer matrix. The higher hydrophilicity and small surface area of the particles greatly improve electrolyte wettability and uptake, while their inorganic nature can eliminate thermal shrinkage observed in pristine polymer separators.[106] Inorganic particles such as aluminum oxide ($Al_2O_3$) and silicon dioxide ($SiO_2$) have been commonly utilized for this application.[88,107] When coated on the surface of polyolefin microporous membranes, a hydrophilic binder is also needed to ensure that the coating integrity is maintained, and the particle properties are not diminished. A common issue with particle coating methods is delamination of the coating from the base separator. Also, the coating inherently decreases the overall porosity and increases the thickness of the membrane. Incorporating the inorganic particles as a filler in polymer matrix overcomes these issues and has also been extensively studied. These composite membranes can be simply formed through solution casting and phase inversion methods to form composite microporous membranes. For example, PVDF[108], PVDF-HFP[109], and high density polyethylene[110] have been used for inorganic particle-filled composite microporous separators. These membranes exhibit the same benefits as the

coated composite separators compared to traditional microporous membranes, without the thickness and porosity penalties. Inorganic particles have also been incorporated into non-woven membranes, typically through particle-filler methods. The improved properties of non-woven membranes further enhance composite separator performance. Inorganic particles can simply be dispersed into polymer solutions before forming the nonwoven mat to incorporate particles into and on the surface of fibers. Electrospinning has been used to incorporate $SiO_2$, $BaTiO_3$, and $Al_2O_3$ particles into PVDF-HFP fiber mats.[107,111] The combination of hydrophilic inorganic fillers and non-woven separator resulted in very high electrolyte uptake and thermal stability, improved ionic conductivity, and stable electrochemical performance. Inorganic particles have also been incorporated into polyimide[112,113] and PVDF[114] non-woven membranes with similar results. Introducing ceramic precursors into the polymer fibers allows for in-situ generation of co-continuous ceramic domains and fiber coatings, circumventing possible issues of particle aggregation or delamination.[115–117]

## 1.3 Electrospinning and Electrospraying

Electrospinning and electrospraying are popular methods to form nanostructured materials. The working principle is that when electrostatic forces overcome the surface tension of a liquid/solution, either a jet or spray is ejected from the surface. A typical setup involves a high voltage source attached to a spinneret. As solution is pumped through the spinneret there is a charge build up due to the applied voltage. At the tip of the spinneret, a Taylor cone of solution forms as the electrostatic forces build up further. When those forces overcome the surface tension, fibers or spray are ejected

from the surface and travel to a grounded collector. Fig. 1.2 shows a typical setup for electrospinning, which is essentially the same for electrospraying but with a different solution.

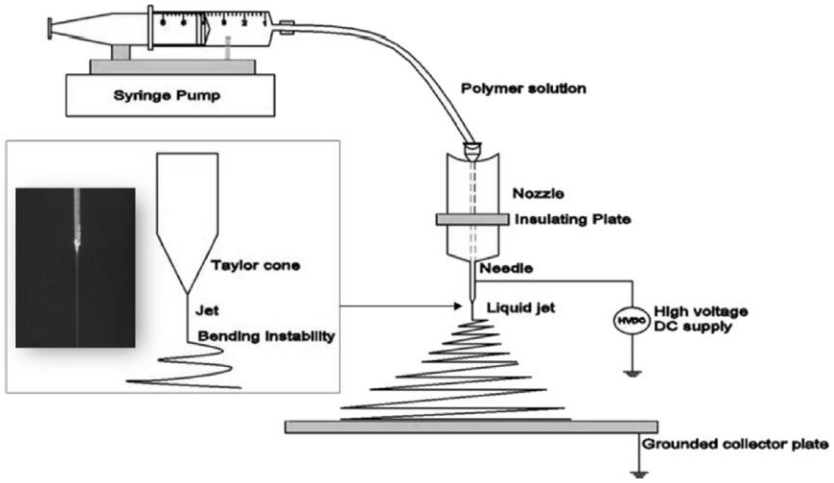


**Figure 1.2.** Typical setup for an electrospinning process.[118]

Parameters such as solution concentration (viscosity), applied voltage, spinneret tip-to-collector distance, and solution feed rate are critical in determining the resultant morphology deposited on the collector. These parameters must be optimized for different solutions to get the desired structures. A viscoelastic polymer solution is used in electrospinning. The polymer molecular weight must be high enough to ensure chain overlap and entanglement, thus forming continuous nanofiber structures. As the fiber jet is ejected from the Taylor cone, bending instabilities ensue from the charged fiber surfaces repelling each other, stretching the fibers to even smaller diameters. Solution solvent is also evaporated as the fiber thins and travels to the collector, depositing a dry non-woven fiber mat. Electrospinning is a facile and versatile method

to form nanofiber separators for battery applications and is therefore applied in this work.

For electrospraying, a wide variety of solutions can be used since only droplets need to be formed. It is convenient for spray-coating materials onto the surface of various substrates, such as non-woven mats.[69,114] Since the solvent evaporates as the charged droplets propel towards the collector, the resulting coating can be completely dry on impact. This expedites material processing as an extra drying step is no longer needed. Electrospraying has been utilized in many battery applications, including separator coatings and electrode fabrication.

## References


(1) Bilgen, S. Structure and Environmental Impact of Global Energy Consumption. *Renew. Sustain. Energy Rev.* **2014**, *38*, 890–902. https://doi.org/10.1016/j.rser.2014.07.004.

(2) Smil, V. *Energy Transitions: Global and National Perspectives*; 2017.

(3) Covert, T. R.; Greenstone, M.; Knittel, C. R. *Will We Ever Stop Using Fossil Fuels?*; 2016; Vol. 30. https://doi.org/10.2139/ssrn.2720633.

(4) Ang, B. W.; Su, B. Carbon Emission Intensity in Electricity Production: A Global Analysis. *Energy Policy* **2016**, *94*, 56–63. https://doi.org/10.1016/j.enpol.2016.03.038.

(5) Neubauer, J.; Pesaran, A.; Bae, C.; Elder, R.; Cunningham, B. Updating United States Advanced Battery Consortium and Department of Energy Battery Technology Targets for Battery Electric Vehicles. *J. Power Sources* **2014**, *271*, 614–621. https://doi.org/10.1016/j.jpowsour.2014.06.043.

(6) Nykvist, B.; Nilsson, M. Rapidly Falling Costs of Battery Packs for Electric Vehicles. *Nat. Clim. Chang.* **2015**, *5* (4), 329–332. https://doi.org/10.1038/nclimate2564.

(7) Nykvist, B.; Sprei, F.; Nilsson, M. Assessing the Progress toward Lower Priced Long Range Battery Electric Vehicles. *Energy Policy* **2019**, *124* (October 2018), 144–155. https://doi.org/10.1016/j.enpol.2018.09.035.

(8) Santillana, G. de. Alessandro Volta. *Sci. Am.* **1965**, *212* (1), 82–91.

(9) Cope, R. C.; Podrazhansky, Y. The Art of Battery Charging. In *Battery Conference on Applications and Advances*; 1999; pp 233–235. https://doi.org/10.1109/bcaa.1999.795996.

(10) Scrosati, B. History of Lithium Batteries. *J. Solid State Electrochem.* **2011**, *15* (7–8), 1623–1630. https://doi.org/10.1007/s10008-011-1386-8.

(11) Kurzweil, P. Gaston Planté and His Invention of the Lead-Acid Battery-The Genesis of the First Practical Rechargeable Battery. *J. Power Sources* **2010**, *195* (14), 4424–4434. https://doi.org/10.1016/j.jpowsour.2009.12.126.

(12) Jung, J. Lead-Acid Battery Technologies: Findamentals, Materials, and Applications. In *Lead-Acid Battery Technologies: Fundamentals, Materials, and Applications*; CRC Press, 2015; pp 3–10.

(13) Jungner, E. W. Swedish Patent. 10177, 1899.

(14) Jungner, E. W. Swedish Patent. 11487, 1899.

(15) Putois, F. Market for Nickel-Cadmium Batteries. *J. Power Sources* **1995**, *57* (1–2), 67–70. https://doi.org/10.1016/0378-7753(95)02243-0.

(16) Li, J.; Xu, Z.; Huang, K. A Novel Process for Recovering Valuable Metals from Waste Nickel - Cadmium Batteries. *Environ. Sci. Technol.* **1967**, *43* (23), 8974–8978.

(17) Ono, K. Past and Future Cadmium Emissions from Municipal Solid-Waste Incinerators in Japan for the Assessment of Cadmium Control Policy. *J. Hazard. Mater.* **2013**, *262*, 741–747. https://doi.org/10.1016/j.jhazmat.2013.09.033.

(18) Tarakina, N. V; Verberck, B. A Portrait of Cadmium. *Nature Chemistry*. Nature Publishing Group 2016, p 96. https://doi.org/10.1038/nchem.2699.

(19) Hong, K. The Development of Hydrogen Storage Alloys and the Progress of Nickel Hydride Batteries. *J. Alloys Compd.* **2001**, *321* (2), 307–313. https://doi.org/10.1016/S0925-8388(01)00957-4.
(20) Sakai, T. Effects of Microencapsulation of Hydrogen Storage Alloy on the Performances of Sealed Nickel/Metal Hydride Batteries. *J. Electrochem. Soc.* **2006**, *134* (3), 558. https://doi.org/10.1149/1.2100509.
(21) Sakai, T.; Yuasa, A.; Ishikawa, H.; Miyamura, H.; Kuriyama, N. Nickel-Metal Hydride Battery Using Microencapsulated Alloys. *J. Less-Common Met.* **1991**, *172–174* (PART 3), 1194–1204. https://doi.org/10.1016/S0022-5088(06)80027-5.
(22) Ovshinsky, S. R.; Fetcenko, M. A.; Ross, J. A Nickel Metal Hydride Battery for Electric Vehicles. *Science (80-. ).* **1993**, *260* (5105), 176–181. https://doi.org/10.1126/science.260.5105.176.
(23) Young, K. Research in Nickel/Metal Hydride Batteries 2017. *Batteries* **2018**, *4* (1), 9. https://doi.org/10.3390/batteries4010009.
(24) Yang, C. C.; Wang, C. C.; Li, M. M.; Jiang, Q. A Start of the Renaissance for Nickel Metal Hydride Batteries: A Hydrogen Storage Alloy Series with an Ultra-Long Cycle Life. *J. Mater. Chem. A* **2017**, *5* (3), 1145–1152. https://doi.org/10.1039/C6TA09736G.
(25) Young, K.; Ng, K.; Bendersky, L. A Technical Report of the Robust Affordable Next Generation Energy Storage System-BASF Program. *Batteries* **2016**, *2* (1), 2. https://doi.org/10.3390/batteries2010002.
(26) Xu, W.; Wang, J.; Ding, F.; Chen, X.; Nasybulin, E.; Zhang, Y.; Zhang, J. G. Lithium Metal Anodes for Rechargeable Batteries. *Energy Environ. Sci.* **2014**, *7* (2), 513–537. https://doi.org/10.1039/c3ee40795k.
(27) Lin, D.; Liu, Y.; Cui, Y. Reviving the Lithium Metal Anode for High-Energy Batteries. *Nat. Nanotechnol.* **2017**, *12* (3), 194–206. https://doi.org/10.1038/nnano.2017.16.
(28) Whittingham, M. S. Electrical Energy Storage and Intercalation Chemistry. *Science (80-. ).* **1976**, *192* (4244), 1126–1127. https://doi.org/10.1126/science.192.4244.1126.
(29) Zachman, M. J.; Tu, Z.; Choudhury, S.; Archer, L. A.; Kourkoutis, L. F. Cryo-STEM Mapping of Solid–Liquid Interfaces and Dendrites in Lithium-Metal Batteries. *Nature*. Springer US 2018, pp 345–349. https://doi.org/10.1038/s41586-018-0397-3.
(30) Harry, K. J.; Hallinan, D. T.; Parkinson, D. Y.; Macdowell, A. A.; Balsara, N. P. Dendrites Formed on Cycled Lithium Metal Electrodes. *Nat. Mater.* **2013**, *13* (1), 69–73. https://doi.org/10.1038/nmat3793.
(31) Tarascon, J. M.; Armand, M. Issues and Challenges Facing Rechargeable Lithium Batteries. *Nature* **2001**, *414* (6861), 359–367. https://doi.org/10.1038/35104644.
(32) Mizushima, K.; Jones, P. C.; Wiseman, P. J.; Goodenough, J. B. Lixcoo2 (O Less-Than X Less-Than-or-Equal-To 1) - a New Cathode Material for Batteries of High-Energy Density. *Mater. Res. Bull.* **1980**, *15* (6), 783–789. https://doi.org/10.1016/0167-2738(81)90077-1.

(33) Whittingham, M. S. History, Evolution, and Future Status of Energy Storage. In *Proceedings of the IEEE*; IEEE, 2012; Vol. 100, pp 1518–1534. https://doi.org/10.1109/JPROC.2012.2190170.
(34) Armand, M.; Tarascon, J. Building Better Batteries. *Nature* **2008**, *451* (February), 652–657.
(35) Diouf, B.; Pode, R. Potential of Lithium-Ion Batteries in Renewable Energy. *Renew. Energy* **2015**, *76*, 375–380. https://doi.org/10.1016/j.renene.2014.11.058.
(36) Nitta, N.; Wu, F.; Lee, J. T.; Yushin, G. Li-Ion Battery Materials: Present and Future. *Mater. Today* **2015**, *18* (5), 252–264. https://doi.org/10.1016/j.mattod.2014.10.040.
(37) Wu, H.; Cui, Y. Designing Nanostructured Si Anodes for High Energy Lithium Ion Batteries. *Nano Today* **2012**, *7* (5), 414–429.
(38) Szczech, J. R.; Jin, S. Nanostructured Silicon for High Capacity Lithium Battery Anodes. *Energy Environ. Sci.* **2011**, *4* (1), 56–72. https://doi.org/10.1039/c0ee00281j.
(39) Scrosati, B.; Garche, J. Lithium Batteries: Status, Prospects and Future. *Journal of Power Sources*. 2010, pp 2419–2430. https://doi.org/10.1016/j.jpowsour.2009.11.048.
(40) Luntz, A. C.; McCloskey, B.; Scheffler, R.; Speidel, A.; Bethune, D. S.; Shelby, R. M. On the Efficacy of Electrocatalysis in Nonaqueous Li-O2 Batteries. *J. Am. Chem. Soc.* **2011**, *133* (45), 18038–18041. https://doi.org/10.1021/ja207229n.
(41) Elia, G. A.; Hassoun, J.; Scrosati, B.; Mueller, F.; Bresser, D.; Passerini, S.; Oberhumer, P.; Tsiouvaras, N.; Reiter, J. An Advanced Lithium − Air Battery Exploiting an Ionic Liquid-Based Electrolyte. *Nano Lett.* **2014**, *14* (11), 6572–6577. https://doi.org/10.1021/nl5031985.
(42) Xiao, J.; Mei, D.; Li, X.; Xu, W.; Wang, D.; Gra, G. L.; Bennett, W. D.; Nie, Z.; Saraf, L. V; Aksay, I. A.; et al. Hierarchically Porous Graphene as a Lithium-Air Battery Electrode. *Nano Lett.* **2011**, *11* (11), 5071–5078. https://doi.org/10.1021/nl203332e.
(43) Tran, C.; Yang, X.; Qu, D. Investigation of the Gas-Diffusion-Electrode Used as Lithium/Air Cathode in Non-Aqueous Electrolyte and the Importance of Carbon Material Porosity. *J. Power Sources* **2010**, *195* (7), 2057–2063. https://doi.org/10.1016/j.jpowsour.2009.10.012.
(44) Balaish, M.; Kraytsberg, A.; Ein-Eli, Y. A Critical Review on Lithium–Air Battery Electrolytes. *Phys. Chem. Chem. Phys.* **2014**, *16* (7), 2801. https://doi.org/10.1039/c3cp54165g.
(45) Veith, G. M.; Dudney, N. J.; Howe, J.; Nanda, J. Spectroscopic Characterization of Solid Discharge Products in Li-Air Cells with Aprotic Carbonate Electrolytes. *J. Phys. Chem. C* **2011**, *115* (29), 14325–14333. https://doi.org/10.1021/jp2043015.
(46) Xu, W.; Xu, K.; Viswanathan, V. V; Towne, S. A.; Hardy, J. S.; Xiao, J.; Nie, Z.; Hu, D.; Wang, D.; Zhang, J. Reaction Mechanisms for the Limited Reversibility of Li – O 2 Chemistry in Organic Carbonate Electrolytes. *J.*

*Power Sources* **2011**, *196* (22), 9631–9639. https://doi.org/10.1016/j.jpowsour.2011.06.099.
(47) Yin, Y. X.; Xin, S.; Guo, Y. G.; Wan, L. J. Lithium-Sulfur Batteries: Electrochemistry, Materials, and Prospects. *Angewandte Chemie - International Edition*. 2013, pp 13186–13200. https://doi.org/10.1002/anie.201304762.
(48) Ceccotti, S. P.; Morris, R. J.; Messick, D. L. A Global Overview of the Sulphur Situation: Industry's Background, Market Trends, and Commercial Aspects of Sulphur Fertilizers. In *Sulphur in Agroecosystems*; Schnug, E., Ed.; Springer Netherlands: Dordrecht, 1998; pp 175–202. https://doi.org/10.1007/978-94-011-5100-9_6.
(49) Manthiram, A.; Fu, Y.; Su, Y. S. Challenges and Prospects of Lithium-Sulfur Batteries. *Acc. Chem. Res.* **2013**, *46* (5), 1125–1134. https://doi.org/10.1021/ar300179v.
(50) Bresser, D.; Passerini, S.; Scrosati, B. Recent Progress and Remaining Challenges in Sulfur-Based Lithium Secondary Batteries - a Review. *Chem. Commun.* **2013**, *49* (90), 10545–10562. https://doi.org/10.1039/c3cc46131a.
(51) Zheng, D.; Zhang, X.; Wang, J.; Qu, D.; Yang, X.; Qu, D. Reduction Mechanism of Sulfur in Lithium-Sulfur Battery: From Elemental Sulfur to Polysulfide. *J. Power Sources* **2016**, *301*, 312–316. https://doi.org/10.1016/j.jpowsour.2015.10.002.
(52) Ellis, B. L.; Lee, K. T.; Nazar, L. F. Positive Electrode Materials for Li-Ion and Li-Batteries. *Chem. Mater.* **2010**, *22* (3), 691–714. https://doi.org/10.1021/cm902696j.
(53) Borchardt, L.; Oschatz, M.; Kaskel, S. Carbon Materials for Lithium Sulfur Batteries - Ten Critical Questions. *Chem. - A Eur. J.* **2016**, *22* (22), 7324–7351. https://doi.org/10.1002/chem.201600040.
(54) Fan, X.; Sun, W.; Meng, F.; Xing, A.; Liu, J. Advanced Chemical Strategies for Lithium–Sulfur Batteries: A Review. *Green Energy and Environment*. Elsevier Ltd 2018, pp 2–19. https://doi.org/10.1016/j.gee.2017.08.002.
(55) Rauh, R. D.; Shuker, F. S.; Marston, J. M.; Brummer, S. B. Formation of Lithium Polysulfides in Ionic Liquids. *J. Inorg. Nucl. Chem.* **1977**, *39* (10), 1761–1766.
(56) Bruce, P. G.; Freunberger, S. A.; Hardwick, L. J.; Tarascon, J. M. Li-O2 and Li-S Batteries with High Energy Storage. *Nature Materials*. December 15, 2012, pp 19–29. https://doi.org/10.1038/nmat3191.
(57) Rosenman, A.; Markevich, E.; Salitra, G.; Aurbach, D.; Garsuch, A.; Chesneau, F. F. Review on Li-Sulfur Battery Systems: An Integral Perspective. *Adv. Energy Mater.* **2015**, *5* (16), 1–21. https://doi.org/10.1002/aenm.201500212.
(58) Liang, X.; Wen, Z.; Liu, Y.; Wu, M.; Jin, J.; Zhang, H.; Wu, X. Improved Cycling Performances of Lithium Sulfur Batteries with LiNO3-Modified Electrolyte. *J. Power Sources* **2011**, *196* (22), 9839–9843. https://doi.org/10.1016/j.jpowsour.2011.08.027.
(59) Zhang, L.; Ling, M.; Feng, J.; Mai, L.; Liu, G.; Guo, J. The Synergetic Interaction between LiNO3 and Lithium Polysulfides for Suppressing Shuttle Effect of Lithium-Sulfur Batteries. *Energy Storage Mater.* **2018**, *11*, 24–29.

https://doi.org/10.1016/j.ensm.2017.09.001.
(60) Adams, B. D.; Carino, E. V; Connell, J. G.; Han, K. S.; Cao, R.; Chen, J.; Zheng, J.; Li, Q.; Mueller, K. T.; Henderson, W. A.; et al. Long Term Stability of Li-S Batteries Using High Concentration Lithium Nitrate Electrolytes. *Nano Energy* **2017**, *40*, 607–617. https://doi.org/10.1016/j.nanoen.2017.09.015.
(61) Ji, X.; Lee, K. T.; Nazar, L. F. A Highly Ordered Nanostructured Carbon-Sulphur Cathode for Lithium-Sulphur Batteries. *Nat. Mater.* **2009**, *8* (6), 500–506. https://doi.org/10.1038/nmat2460.
(62) Dörfler, S.; Hagen, M.; Althues, H.; Tübke, J.; Kaskel, S.; Hoffmann, M. J. High Capacity Vertical Aligned Carbon Nanotube/Sulfur Composite Cathodes for Lithium-Sulfur Batteries. *Chem. Commun.* **2012**, *48* (34), 4097–4099. https://doi.org/10.1039/c2cc17925c.
(63) Guo, J.; Xu, Y.; Wang, C. Sulfur-Impregnated Disordered Carbon Nanotubes Cathode for Lithium-Sulfur Batteries. *Nano Lett.* **2011**, *11* (10), 4288–4294. https://doi.org/10.1021/nl202297p.
(64) Gueon, D.; Hwang, J. T.; Yang, S. B.; Cho, E.; Sohn, K.; Yang, D. K.; Moon, J. H. Spherical Macroporous Carbon Nanotube Particles with Ultrahigh Sulfur Loading for Lithium-Sulfur Battery Cathodes. *ACS Nano* **2018**, *12* (1), 226–233. https://doi.org/10.1021/acsnano.7b05869.
(65) Schuster, J.; He, G.; Mandlmeier, B.; Yim, T.; Lee, K. T.; Bein, T.; Nazar, L. F. Spherical Ordered Mesoporous Carbon Nanoparticles with High Porosity for Lithium-Sulfur Batteries. *Angew. Chemie - Int. Ed.* **2012**, *51* (15), 3591–3595. https://doi.org/10.1002/anie.201107817.
(66) Song, J.; Xu, T.; Gordin, M. L.; Zhu, P.; Lv, D.; Jiang, Y. B.; Chen, Y.; Duan, Y.; Wang, D. Nitrogen-Doped Mesoporous Carbon Promoted Chemical Adsorption of Sulfur and Fabrication of High-Areal-Capacity Sulfur Cathode with Exceptional Cycling Stability for Lithium-Sulfur Batteries. *Adv. Funct. Mater.* **2014**, *24* (9), 1243–1250. https://doi.org/10.1002/adfm.201302631.
(67) Zhang, X. Q.; He, B.; Li, W. C.; Lu, A. H. Hollow Carbon Nanofibers with Dynamic Adjustable Pore Sizes and Closed Ends as Hosts for High-Rate Lithium-Sulfur Battery Cathodes. *Nano Res.* **2018**, *11* (3), 1238–1246. https://doi.org/10.1007/s12274-017-1737-6.
(68) Zheng, G.; Yang, Y.; Cha, J. J.; Hong, S. S.; Cui, Y. Hollow Carbon Nanofiber-Encapsulated Sulfur Cathodes for High Specific Capacity Rechargeable Lithium Batteries. *Nano Lett.* **2011**, *11* (10), 4462–4467. https://doi.org/10.1021/nl2027684.
(69) Lee, J.; Ko, B.; Kang, J.; Chung, Y.; Kim, Y.; Halim, W.; Lee, J. H.; Joo, Y. L. Facile and Scalable Fabrication of Highly Loaded Sulfur Cathodes and Lithium–Sulfur Pouch Cells via Air-Controlled Electrospray. *Mater. Today Energy* **2017**, *6*, 255–263. https://doi.org/10.1016/j.mtener.2017.11.003.
(70) Ji, L.; Rao, M.; Zheng, H.; Zhang, L.; Li, Y.; Duan, W.; Guo, J.; Cairns, E. J.; Zhang, Y. Graphene Oxide as a Sulfur Immobilizer in High Performance Lithium/Sulfur Cells. *J. Am. Chem. Soc.* **2011**, *133* (46), 18522–18525. https://doi.org/10.1021/ja206955k.
(71) Chen, K.; Cao, J.; Lu, Q.; Wang, Q.; Yao, M.; Han, M.; Niu, Z.; Chen, J. Sulfur

Nanoparticles Encapsulated in Reduced Graphene Oxide Nanotubes for Flexible Lithium-Sulfur Batteries. *Nano Res.* **2018**, *11* (3), 1345–1357. https://doi.org/10.1007/s12274-017-1749-2.

(72) Wang, H.; Yang, Y.; Liang, Y.; Robinson, J. T.; Li, Y.; Jackson, A.; Cui, Y.; Dai, H. Graphene-Wrapped Sulfur Particles as a Rechargeable Lithium-Sulfur Battery Cathode Material with High Capacity and Cycling Stability. *Nano Lett.* **2011**, *11* (7), 2644–2647. https://doi.org/10.1021/nl200658a.

(73) Huang, J. Q.; Zhang, Q.; Wei, F. Multi-Functional Separator/Interlayer System for High-Stable Lithium-Sulfur Batteries: Progress and Prospects. *Energy Storage Mater.* **2015**, *1*, 127–145. https://doi.org/10.1016/j.ensm.2015.09.008.

(74) Deng, N.; Kang, W.; Liu, Y.; Ju, J.; Wu, D.; Li, L.; Hassan, B. S.; Cheng, B. A Review on Separators for Lithium-Sulfur Battery: Progress and Prospects. *J. Power Sources* **2016**, *331*, 132–155. https://doi.org/10.1016/j.jpowsour.2016.09.044.

(75) Rana, M.; Li, M.; Huang, X.; Luo, B.; Gentle, I.; Knibbe, R. Recent Advances in Separators to Mitigate Technical Challenges Associated with Re-Chargeable Lithium Sulfur Batteries. *J. Mater. Chem. A* **2019**, *7* (12), 6596–6615. https://doi.org/10.1039/c8ta12066h.

(76) Fan, C. Y.; Yuan, H. Y.; Li, H. H.; Wang, H. F.; Li, W. L.; Sun, H. Z.; Wu, X. L.; Zhang, J. P. The Effective Design of a Polysulfide-Trapped Separator at the Molecular Level for High Energy Density Li-S Batteries. *ACS Appl. Mater. Interfaces* **2016**, *8* (25), 16108–16115. https://doi.org/10.1021/acsami.6b04578.

(77) Lu, Y.; Gu, S.; Guo, J.; Rui, K.; Chen, C.; Zhang, S.; Jin, J.; Yang, J.; Wen, Z. Sulfonic Groups Originated Dual-Functional Interlayer for High Performance Lithium-Sulfur Battery. *ACS Appl. Mater. Interfaces* **2017**, *9* (17), 14878–14888. https://doi.org/10.1021/acsami.7b02142.

(78) Su, Y. S.; Manthiram, A. A New Approach to Improve Cycle Performance of Rechargeable Lithium-Sulfur Batteries by Inserting a Free-Standing MWCNT Interlayer. *Chem. Commun.* **2012**, *48* (70), 8817–8819. https://doi.org/10.1039/c2cc33945e.

(79) Lee, J. H.; Kang, J.; Kim, S. W.; Halim, W.; Frey, M. W.; Joo, Y. L. Effective Suppression of the Polysulfide Shuttle Effect in Lithium-Sulfur Batteries by Implementing RGO-PEDOT:PSS-Coated Separators via Air-Controlled Electrospray. *ACS Omega* **2018**, *3* (12), 16465–16471. https://doi.org/10.1021/acsomega.8b02551.

(80) Bauer, I.; Thieme, S.; Brückner, J.; Althues, H.; Kaskel, S. Reduced Polysulfide Shuttle in Lithium-Sulfur Batteries Using Nafion-Based Separators. *J. Power Sources* **2014**, *251*, 417–422. https://doi.org/10.1016/j.jpowsour.2013.11.090.

(81) Huang, J. Q.; Zhang, Q.; Peng, H. J.; Liu, X. Y.; Qian, W. Z.; Wei, F. Ionic Shield for Polysulfides towards Highly-Stable Lithium-Sulfur Batteries. *Energy Environ. Sci.* **2014**, *7* (1), 347–353. https://doi.org/10.1039/c3ee42223b.

(82) Arora, P.; Zhang, Z. Battery Separators. *Chem. Rev.* **2004**, *104* (10), 4419–4462. https://doi.org/10.1021/cr020738u.

(83) Love, C. T. Thermomechanical Analysis and Durability of Commercial Micro-Porous Polymer Li-Ion Battery Separators. *J. Power Sources* **2011**, *196* (5),

2905–2912. https://doi.org/10.1016/j.jpowsour.2010.10.083.
(84) Jung, B.; Lee, B.; Jeong, Y. C.; Lee, J.; Yang, S. R.; Kim, H.; Park, M. Thermally Stable Non-Aqueous Ceramic-Coated Separators with Enhanced Nail Penetration Performance. *J. Power Sources* **2019**, *427* (December 2018), 271–282. https://doi.org/10.1016/j.jpowsour.2019.04.046.
(85) Wang, Q.; Ping, P.; Zhao, X.; Chu, G.; Sun, J.; Chen, C. Thermal Runaway Caused Fire and Explosion of Lithium Ion Battery. *J. Power Sources* **2012**, *208* (June 2012), 210–224. https://doi.org/10.1016/j.jpowsour.2012.02.038.
(86) Feng, X.; Ouyang, M.; Liu, X.; Lu, L.; Xia, Y.; He, X. Thermal Runaway Mechanism of Lithium Ion Battery for Electric Vehicles: A Review. *Energy Storage Materials*. Elsevier B.V. 2018, pp 246–267. https://doi.org/10.1016/j.ensm.2017.05.013.
(87) Lee, H.; Yanilmaz, M.; Toprakci, O.; Fu, K.; Zhang, X. A Review of Recent Developments in Membrane Separators for Rechargeable Lithium-Ion Batteries. *Energy Environ. Sci.* **2014**, *7* (12), 3857–3886. https://doi.org/10.1039/c4ee01432d.
(88) Zhang, S. S. A Review on the Separators of Liquid Electrolyte Li-Ion Batteries. *Journal of Power Sources*. 2007, pp 351–364. https://doi.org/10.1016/j.jpowsour.2006.10.065.
(89) Song, J. Y.; Wang, Y. Y.; Wan, C. C. Conductivity Study of Porous Plasticized Polymer Electrolytes Based on Poly(Vinylidene Fluoride) A Comparison with Polypropylene Separators. *J. Electrochem. Soc.* **2002**, *147* (9), 3219. https://doi.org/10.1149/1.1393886.
(90) Huai, Y.; Gao, J.; Deng, Z.; Suo, J. Preparation and Characterization of a Special Structural Poly(Acrylonitrile)-Based Microporous Membrane for Lithium-Ion Batteries. *Ionics (Kiel)*. **2010**, *16* (7), 603–611. https://doi.org/10.1007/s11581-010-0431-4.
(91) Min, H.; Ko, J.; Kim, D. Preparation and Characterization of Porous Polyacrylonitrile Membranes for Lithium-Ion Polymer Batteries. *J. Power Sources* **2003**, *119–121*, 469–472. https://doi.org/10.1016/s0378-7753(03)00206-4.
(92) Saunier, J.; Alloin, F.; Sanchez, J. Y.; Caillon, G. Thin and Flexible Lithium-Ion Batteries: Investigation of Polymer Electrolytes. *J. Power Sources* **2003**, *119–121*, 454–459. https://doi.org/10.1016/S0378-7753(03)00197-6.
(93) Ko, J. M.; Min, E. G.; Kim, D. W.; Ryu, K. S.; Kim, K. M.; Lee, Y. G.; Chang, S. H. Thin-Film Type Li-Ion Battery, Using a Polyethylene Separator Grafted with Glycidyl Methacrylate. *Electrochim. Acta* **2004**, *50* (2-3 SPEC. ISS.), 367–370. https://doi.org/10.1016/j.electacta.2004.01.127.
(94) Kim, K. J.; Kim, Y. H.; Song, J. H.; Jo, Y. N.; Kim, J. S.; Kim, Y. J. Effect of Gamma Ray Irradiation on Thermal and Electrochemical Properties of Polyethylene Separator for Li Ion Batteries. *J. Power Sources* **2010**, *195* (18), 6075–6080. https://doi.org/10.1016/j.jpowsour.2009.12.056.
(95) Kim, J. Y.; Lee, Y.; Lim, D. Y. Plasma-Modified Polyethylene Membrane as a Separator for Lithium-Ion Polymer Battery. *Electrochim. Acta* **2009**, *54* (14), 3714–3719. https://doi.org/10.1016/j.electacta.2009.01.055.

(96) Ju, H.; Li, Z.; Ju, L.; Xu, Y. Methyl Methacrylate (MMA)-Grafted Polypropylene (PP) Separator for Rechargeable Lithium Metal Battery. *ECS Electrochem. Lett.* **2012**, *1* (4), A59–A62. https://doi.org/10.1149/2.008203eel.
(97) Park, J. H.; Park, W.; Kim, J. H.; Ryoo, D.; Kim, H. S.; Jeong, Y. U.; Kim, D. W.; Lee, S. Y. Close-Packed Poly(Methyl Methacrylate) Nanoparticle Arrays-Coated Polyethylene Separators for High-Power Lithium-Ion Polymer Batteries. *J. Power Sources* **2011**, *196* (16), 7035–7038. https://doi.org/10.1016/j.jpowsour.2010.09.102.
(98) Xiong, M.; Tang, H.; Wang, Y.; Pan, M. Ethylcellulose-Coated Polyolefin Separators for Lithium-Ion Batteries with Improved Safety Performance. *Carbohydr. Polym.* **2014**, *101* (1), 1140–1146. https://doi.org/10.1016/j.carbpol.2013.10.073.
(99) Liao, H.; Zhang, H.; Hong, H.; Li, Z.; Qin, G.; Zhu, H.; Lin, Y. Novel Cellulose Aerogel Coated on Polypropylene Separators as Gel Polymer Electrolyte with High Ionic Conductivity for Lithium-Ion Batteries. *J. Memb. Sci.* **2016**, *514*, 332–339. https://doi.org/10.1016/j.memsci.2016.05.009.
(100) Jeong, Y. B.; Kim, D. W. Effect of Thickness of Coating Layer on Polymer-Coated Separator on Cycling Performance of Lithium-Ion Polymer Cells. *J. Power Sources* **2004**, *128* (2), 256–262. https://doi.org/10.1016/j.jpowsour.2003.09.073.
(101) Ryou, M.; Lee, D. J.; Lee, J.-N.; Lee, Y. M.; Park, J.; Choi, J. W. Lithium-Ion Batteries: Excellent Cycle Life of Lithium-Metal Anodes in Lithium-Ion Batteries with Mussel-Inspired Polydopamine-Coated Separators (Adv. Energy Mater. 6/2012). *Adv. Energy Mater.* **2012**, *2* (6), 610–610. https://doi.org/10.1002/aenm.201290031.
(102) Chen, W.; Liu, Y.; Ma, Y.; Liu, J.; Liu, X. Improved Performance of PVdF-HFP/PI Nanofiber Membrane for Lithium Ion Battery Separator Prepared by a Bicomponent Cross-Electrospinning Method. *Mater. Lett.* **2014**, *133*, 67–70. https://doi.org/10.1016/j.matlet.2014.06.163.
(103) Deimede, V.; Elmasides, C. Separators for Lithium-Ion Batteries: A Review on the Production Processes and Recent Developments. *Energy Technol.* **2015**, *3* (5), 453–468. https://doi.org/10.1002/ente.201402215.
(104) Miao, Y. E.; Zhu, G. N.; Hou, H.; Xia, Y. Y.; Liu, T. Electrospun Polyimide Nanofiber-Based Nonwoven Separators for Lithium-Ion Batteries. *J. Power Sources* **2013**, *226* (February 2014), 82–86. https://doi.org/10.1016/j.jpowsour.2012.10.027.
(105) Zhu, J.; Chen, C.; Lu, Y.; Zang, J.; Jiang, M.; Kim, D.; Zhang, X. Highly Porous Polyacrylonitrile/Graphene Oxide Membrane Separator Exhibiting Excellent Anti-Self-Discharge Feature for High-Performance Lithium-Sulfur Batteries. *Carbon N. Y.* **2016**, *101*, 272–280. https://doi.org/10.1016/j.carbon.2016.02.007.
(106) Liu, H.; Xu, J.; Guo, B.; He, X. Effect of Al2O3/SiO2 Composite Ceramic Layers on Performance of Polypropylene Separator for Lithium-Ion Batteries. *Ceram. Int.* **2014**, *40*, 14105–14110. https://doi.org/10.1016/j.ceramint.2014.05.142.

(107) Raghavan, P.; Zhao, X.; Kim, J. K.; Manuel, J.; Chauhan, G. S.; Ahn, J. H.; Nah, C. Ionic Conductivity and Electrochemical Properties of Nanocomposite Polymer Electrolytes Based on Electrospun Poly(Vinylidene Fluoride-Co-Hexafluoropropylene) with Nano-Sized Ceramic Fillers. *Electrochim. Acta* **2008**, *54* (2), 228–234. https://doi.org/10.1016/j.electacta.2008.08.007.
(108) Prasanth, R.; Shubha, N.; Hng, H. H.; Srinivasan, M. Effect of Nano-Clay on Ionic Conductivity and Electrochemical Properties of Poly(Vinylidene Fluoride) Based Nanocomposite Porous Polymer Membranes and Their Application as Polymer Electrolyte in Lithium Ion Batteries. *Eur. Polym. J.* **2013**, *49* (2), 307–318. https://doi.org/10.1016/j.eurpolymj.2012.10.033.
(109) Jeong, H. S.; Hong, S. C.; Lee, S. Y. Effect of Microporous Structure on Thermal Shrinkage and Electrochemical Performance of Al2O3/Poly(Vinylidene Fluoride-Hexafluoropropylene) Composite Separators for Lithium-Ion Batteries. *J. Memb. Sci.* **2010**, *364*, 177–182. https://doi.org/10.1016/j.memsci.2010.08.012.
(110) Park, J. S.; Gwon, S. J.; Lim, Y. M.; Nho, Y. C. Influence of the Stretching Temperature on an Alumina Filled Microporous High Density Polyethylene Membrane. *Mater. Des.* **2010**, *31* (7), 3215–3219. https://doi.org/10.1016/j.matdes.2010.02.020.
(111) Raghavan, P.; Zhao, X.; Manuel, J.; Chauhan, G. S.; Ahn, J. H.; Ryu, H. S.; Ahn, H. J.; Kim, K. W.; Nah, C. Electrochemical Performance of Electrospun Poly(Vinylidene Fluoride-Co-Hexafluoropropylene)-Based Nanocomposite Polymer Electrolytes Incorporating Ceramic Fillers and Room Temperature Ionic Liquid. *Electrochim. Acta* **2010**, *55* (4), 1347–1354. https://doi.org/10.1016/j.electacta.2009.05.025.
(112) Wang, Y.; Wang, S.; Fang, J.; Ding, L. X.; Wang, H. A Nano-Silica Modified Polyimide Nanofiber Separator with Enhanced Thermal and Wetting Properties for High Safety Lithium-Ion Batteries. *J. Memb. Sci.* **2017**, *537* (January), 248–254. https://doi.org/10.1016/j.memsci.2017.05.023.
(113) Shayapat, J.; Chung, O. H.; Park, J. S. Electrospun Polyimide-Composite Separator for Lithium-Ion Batteries. *Electrochim. Acta* **2015**, *170*, 110–121. https://doi.org/10.1016/j.electacta.2015.04.142.
(114) Yanilmaz, M.; Lu, Y.; Dirican, M.; Fu, K.; Zhang, X. Nanoparticle-on-Nanofiber Hybrid Membrane Separators for Lithium-Ion Batteries via Combining Electrospraying and Electrospinning Techniques. *J. Memb. Sci.* **2014**, *456*, 57–65. https://doi.org/10.1016/j.memsci.2014.01.022.
(115) Smith, S. A.; Park, J. H.; Williams, B. P.; Joo, Y. L. Polymer/Ceramic Co-Continuous Nanofiber Membranes via Room-Curable Organopolysilazane for Improved Lithium-Ion Battery Performance. *J. Mater. Sci.* **2017**, *52* (7), 3657–3669. https://doi.org/10.1007/s10853-016-0574-4.
(116) Smith, S. A.; Williams, B. P.; Joo, Y. L. Effect of Polymer and Ceramic Morphology on the Material and Electrochemical Properties of Electrospun PAN/Polymer Derived Ceramic Composite Nanofiber Membranes for Lithium Ion Battery Separators. *J. Memb. Sci.* **2017**, *526* (December 2016), 315–322. https://doi.org/10.1016/j.memsci.2016.12.052.

(117) Yanilmaz, M.; Lu, Y.; Zhu, J.; Zhang, X. Silica/Polyacrylonitrile Hybrid Nanofiber Membrane Separators via Sol-Gel and Electrospinning Techniques for Lithium-Ion Batteries. *J. Power Sources* **2016**, *313*, 205–212. https://doi.org/10.1016/j.jpowsour.2016.02.089.
(118) Anu Bhushani, J.; Anandharamakrishnan, C. Electrospinning and Electrospraying Techniques: Potential Food Based Applications. *Trends Food Sci. Technol.* **2014**, *38* (1), 21–33. https://doi.org/10.1016/j.tifs.2014.03.004.

# Chapter 2. Polyimide/Ceramic Composite Non-Woven Separators for Lithium-Sulfur Batteries

## 2.1 Introduction

Batteries with high energy density and long cycle life are necessary to power the future of personal electronics, hybrid electric vehicles, and fully electric vehicles. Current commercial lithium-ion (Li-ion) battery chemistries are quickly approaching their practical limits, and better alternatives are necessary.[1,2] One such alternative receiving a lot of attention is the lithium-sulfur (Li-S) chemistry due to its high theoretical specific capacity (1675 mAh/g) and energy density (2600 Wh/kg).[3,4] Furthermore, sulfur is naturally abundant, inexpensive, and environmentally benign.[5] Several issues, including poor active sulfur utilization and the polysulfide shuttle effect, have limited its success and commercialization.

Numerous approaches have been undertaken to overcome the inherent drawbacks of Li-S. One of the most successful for improving sulfur is through using conductive nanostructured carbon materials in the cathodes, which lead to improved sulfur electrical contact. Using lightweight carbons also minimizes the reduction in energy density. Carbon nanofibers,[6–8] carbon nanotubes,[9–12] porous carbon particles,[13–15] graphene oxide (GO),[16,17] and reduced graphene oxide (rGO)[18,19] have all been used to improve discharge capacities through enhanced sulfur utilization and impede the diffusion of soluble higher order polysulfides away from the cathode, especially when the sulfur material is entrapped in the pores of a conductive framework. The addition of an interlayer between the cathode and separator has also been successful in

slowing/preventing soluble polysulfide shuttling through the separator, improving cycle life and Coulombic efficiency.[3,20–22] Both organic and inorganic materials have been used to limit polysulfide shuttling through means of physical blocking and chemical or physical confinement.[22]

Due to these challenges, the bulk of Li-S research has focused on cathode and electrolyte development, with little effort towards novel separators for this system. Separators play an important role in preventing electrical contact between the electrodes while allowing lithium ion transport between them, and therefore largely influence overall kinetics of the battery. Microporous polyolefin membranes are typically employed in lithium batteries due to their stability against lithium metal and good mechanical properties.[23] However, they suffer from low porosity, electrolyte wettability, and electrolyte uptake, which hinder battery performance at higher charge/discharge rates.[24] These polyolefin membranes are also known to shrink at elevated temperatures, leading to short-circuit from electrode contact and possible catastrophic battery failure.[25] Thermally stable glass fiber (GF) membranes have shown promise in lithium-sulfur cells, improving cycling performance especially at higher rates due to their higher porosity and electrolyte uptake.[26–28] GF membranes are typically hundreds of microns in thickness, however, drastically reducing the overall energy density of the cell. Non-woven polyacrylonitrile (PAN)/graphene oxide (GO) separators have also been introduced as a viable alternative separator for Li-S with membrane thicknesses of 65 μm.[29] These separators were able to minimize polysulfide shuttling through favorable interactions of the GO functional groups and PAN nitrile

groups with negatively charged polysulfide anions, and improve high-rate performance with increased porosity and better electrolyte wettability.

For Li-ion, inclusion of inorganic ceramic fillers on the surface or into the matrix of separators has been shown to improve overall mechanical and electrochemical properties. Nanoparticles such as silica and alumina have been applied to both microporous[30,31] and non-woven separators,[32,33] resulting in improved thermal stability and rate performance. Furthermore, adding ceramic precursors directly into electrospinning solutions avoids potential issues with particle delamination, phase separation, and particle aggregation.[34–36]

In this work, a novel polymer/ceramic hybrid non-woven separator was developed using thermally stable polyimide (PI) and a ladder polysilsesquioxane (PSSQ) ceramic for use in lithium-sulfur batteries. These PI/PSSQ separators were fabricated through gas-assisted electrospinning to form nanofiber non-woven mats, with up to 20 wt% PSSQ in the fibers investigated. At this time, these separators are believed to be the thinnest (50 μm) non-woven separators applied to a Li-S system. The PI/PSSQ separators exhibit superior porosity, electrolyte uptake, and ionic conductivity compared to commercial microporous polypropylene due to their fibrous mechanical structure and properties induced by PSSQ inclusion. These separators were thermally stable well above temperatures seen in typical battery abuse conditions and retained their structural integrity even after being ignited, whereas the commercial separator readily shrunk in both cases. In Li-S cells, superior cycling performance was seen at 2C charge/discharge rates, owing to high ionic conductivity through the fibrous structure and favorable electrolyte interactions with PI and PSSQ.

## 2.2 Experimental Methods

### 2.2.1 Preparation of Polyimide/Ceramic Non-Woven Separators via Gas-Assisted Electrospinning

All materials used in this study were purchased from Sigma-Aldrich unless otherwise stated. Polyimide/ceramic hybrid separators were prepared using the gas-assisted electrospinning method. P84 polyimide (Powder, Evonik) was dissolved in N,N-dimethylformamide (DMF) to form a 16 wt% solution for the polymer/ceramic separators and 20 wt% for polyimide only membranes. Each mixture was stirred at 65 °C on a hotplate overnight. The ladder polysilsesquioxane (PSSQ) ceramic used was PMK (DJ Semichem). One hour prior to electrospinning, the solution was removed from the hot plate and PSSQ was added to the desired solid content mass ratio. Ceramic amounts of 0, 5, 10, and 20 solid wt% were investigated. The solution was then stirred at room temperature until the PSSQ was thoroughly dissolved, and vigorously stirred on a vortex mixer for two minutes to ensure a homogeneous mixture before electrospinning. A Harvard Apparatus PHD Ultra was used to electrospin the solution onto an aluminum foil current collector in a chamber controlled at 16 % relative humidity. A coaxial needle with 12-gauge inner needle and 16-gauge outer shell was used. The solution was fed through the inner needle at an infusion rate of 0.03 mL/min, and 16 % RH dry air was supplied through the outer shell at an air pressure of 10 psi. The tip-to-collector distance and applied voltage were 15 cm and 25 kV, respectively. The resulting fiber mat was peeled from the collector and heat treated at 300 °C under air for 3 hours with a 5 °C/min ramp rate. The fiber mat was

then punched into 16 mm diameter discs and cold-calendered to about 50 μm in thickness before use.

### 2.2.2 Material Characterization

Thermal stability of PI was investigated using thermogravimetric analysis (TGA, TA Instruments Q500) with a 10 °C/min temperature ramp rate under air flow. Fourier transform infrared spectroscopy (FTIR, PerkinElmer Frontier) was performed to ensure the removal of the PSSQ acrylate side chains after heat treatment. To study the morphology, diameter, and uniformity of the electrospun fibers, field emission scanning electron microscopy (FESEM, Tescan Mira3) with an accelerating voltage of 5 kV was employed. Membrane pore size distributions were determined using a capillary flow porometer (CFP-1100-AEHXL, Porous Materials Inc.).

Dimensional thermal stability of the separators was determined with a shrinkage test by placing them in a 150 °C oven for two hours under air with a 5 °C/min ramp rate. Flammability of the separator materials was tested by soaking each membrane in electrolyte and lighting the excess electrolyte with a butane torch. For this test, a standard lithium-ion electrolyte consisting of 1 M lithium hexfluorophosphate ($LiPF_6$) in ethylene carbonate/diethyl carbonate/dimethyl carbonate (EC/DEC/DMC, 1/1/1 by vol) was used.

### 2.2.3 Electrochemical Characterization

The Li-S electrolyte used in this study was 1 M lithium bis(trifluoromethane) sulfonimide (LiTFSI) and 1 wt% lithium nitrate ($LiNO_3$) in a 1:1 volume mixture of

1,3-dioxolane (DOL) and 1,2-dimethoxyethane (DME). Electrolyte uptake was determined by soaking the separators in electrolyte for two hours, and calculating the mass change with the equation:

$$Electrolyte\ Uptake\ (\%) = \frac{W_f - W_i}{W_i}\ x\ 100 \quad (2)$$

Where $W_i$ and $W_f$ are the masses of the separator before and after soaking in liquid electrolyte for two hours, respectively.

Ionic conductivity was measured using electrochemical impedance spectroscopy (EIS, Parstat 4000, Princeton Applied Materials). For these tests, separators were soaked with 25 μL of electrolyte to mimic battery cell conditions and sandwiched between two stainless steel discs in a CR2032 coin cell. A frequency range from 100 kHz to 0.1 Hz was applied with an AC amplitude of 10 mV. Ionic conductivity was calculated according to the equation:

$$\sigma = \frac{d}{R_b\ x\ A} \quad (3)$$

Where d is the thickness of the separator, $R_b$ is the bulk resistance, and A is the surface area of the stainless steel electrode (1.96 $cm^2$). $R_b$ is defined as the high frequency intercept of the real axis.

CR2032 coin cells were assembled to tests the electrochemical performance of the polyimide/ceramic separators in Li-S. The slurry cathode used in this study was prepared by first infiltrating sulfur into porous carbons. Active sulfur material (Spectrum Chemical) was mixed with Ketjenblack (KB, EC-600JD, AkzoNobel) at a 3:1 ratio, then grinded and heated at 155 °C for 12 hours in a hydrothermal reactor to melt impregnate the sulfur into the KB. Polyvinylidene fluoride (PVDF) was dissolved

in N-methyl-2-pyrrolidone (NMP) at 10 wt% to serve as the binder. Super C65 (TIMCAL) was used as the conductive carbon. A homogeneous slurry was formed by combining NMP with 70 wt% S/KB, 20 wt% Super C65 and 10 wt% PVDF and mixing for 3 hours in a ball mixer. This was then cast onto aluminum foil with a doctor blade. The slurry was dried at 60 °C under vacuum for 12 hours and punched into 15 mm discs. The mass loading of active sulfur material was between 0.95 to 1.1 $mg/cm^2$. Li-S coin cells were fabricating by placing the separator between the slurry cathode and lithium metal foil. An electrolyte ratio of 15 μL/mg S was added to the separator. Celgard 2400 was used as the reference separator. Coin cells were cycled between 1.8 and 2.8 V vs $Li/Li^+$ using a Landt battery tester. All discharge capacities and current densities are based on active sulfur mass. Current densities were set according to a sulfur theoretical specific capacity of 1675 mAh/g.

## 2.3 Results and Discussion

Polyimides are a class of polymer known for their heat and chemical resistance owing to their rigid aromatic backbone structure.[37] Since gas-assisted electrospinning was employed to fabricate the polyimide nanofiber separators, a soluble form of polyimide was used. The thermal stability of polyimide was characterized by TGA, as shown in Fig. 2.1. Onset of thermal degradation begins after 400 °C, confirming that even though the polyimide used in this work is functionalized to be soluble, it still maintains high temperature stability.

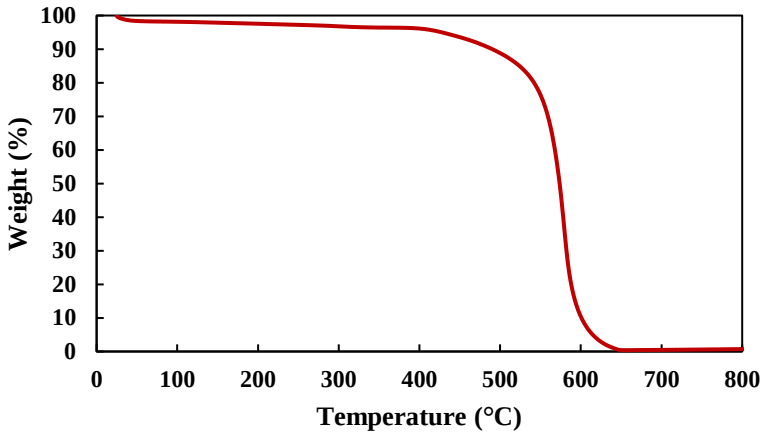


**Figure 2.1.** TGA thermogram of PI material.

PSSQ solubility due to the presence of organic functional groups allows for facile fabrication of polymer/ceramic nanofibers through the electrospinning method, with as high as 20 wt% PSSQ in the fibers presented in this work. The solid nature of soluble PSSQs means there is no time-dependability for the spinning process as there is for room-temperature curable ceramic precursors, further aiding in the overall feasibility of electrospinning these composite fibers. The challenge with these PSSQ materials is that due to their solubility in common polar solvents, they are also soluble in battery electrolytes. To overcome this, a simple heat treatment method was employed to remove the polar acrylate functional group and thus eliminate its solubility in Li-S battery electrolyte. Fig. 2.2 shows the FTIR acrylate peaks for PSSQ before and after heat treatment at 300 °C for 3 hours in air. The absorption peaks at 1716 and 1637 $cm^{-1}$ represent the C=O and C=C bonds of the acrylate functional group, respectively.[38,39] After the heat treatment, the signals for these bonds disappears, confirming the effective removal of this polar soluble functional group in the PSSQ structure. Using

polyimide allows for this method, as typical electrospun non-woven fiber mats are not thermally stable up to the temperatures necessary to remove the functional side chains.

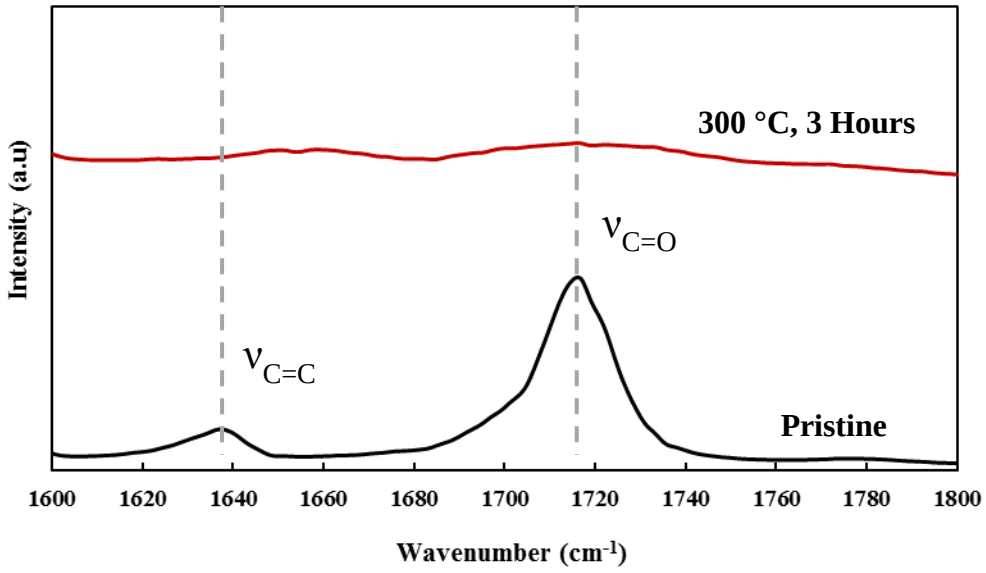


**Figure 2.2.** FTIR spectra showing removal of the acrylate functional group from the Si-O backbone of PSSQ after heat treatment.

Non-calendered fiber morphologies after heat treatment with 0, 5, 10, and 20 wt% PSSQ are shown in Fig. 2.1. Thin nanofibers of PI with and without PSSQ have been obtained through the gas-assisted electrospinning method. Each membrane consists of randomly oriented nanofibers, yielding a highly porous structure. Very similar fiber morphologies were obtained with the various ceramic content, with diameters in the range of 150 – 300 nm for all except the 95/5 PI/PSSQ fibers. For this case, the fiber diameters were smaller, on the order of 75 – 200 nm, and more bead impurities were present in the nanofibers. This is likely due to the lower initial PI solution concentration (16 wt%) used for electrospinning the PI/PSSQ fibers compared to the

pure PI case (20 wt%), while only adding 5 wt% PSSQ relative to the PI. The lower overall solution concentration and viscosity makes it harder for the polymer chains to properly overlap and form continuous nanofibers, thus leading to more prominent bead structures.[40] Overall, no ceramic particles were observed on the surface of the fibers, indicating successful incorporation of the PSSQ into the structure of the fibers.

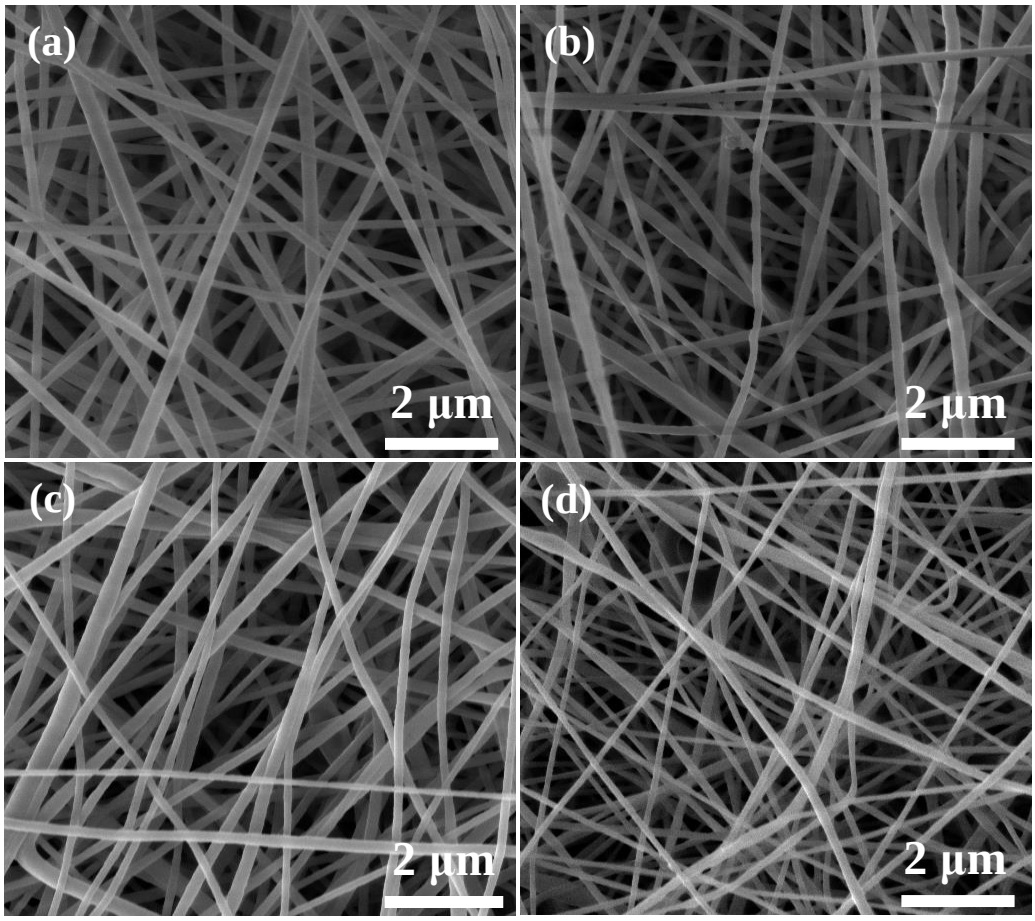


**Figure 2.3.** SEM images of non-woven fiber mats containing: (a) PI only, (b) 95/5 PI/PSSQ, (c) 90/10 PI/PSSQ, and (d) 80/20 PI/PSSQ.

Membrane properties for the various separators are presented in Table 2.1. Electrospun separators exhibit higher porosities than microporous Celgard due to the

large tortuous pore structure from overlapping nanofibers. Mean pore sizes measured by capillary flow porometry indicate that the pores between fibers of the non-woven membranes are small enough to effectively trap electrolyte within the separator. High porosity and small effective pore sizes lead to the ability to hold a large volume of electrolyte compared to the slit-like pores of dry-laid microporous membranes.

Interestingly, there is a trend that as the amount of PSSQ is increased, the electrolyte uptake decreases. This can be explained by the rigidity of the fibers afforded by the addition of PSSQ. Increasing the ceramic content of the fibers reduces the swelling induced by electrolyte filling the membrane pores since the fibers have higher stiffness and cannot move to accommodate higher amounts of liquid. The Si-O backbone of PSSQ materials introduces rigidity into the polymer fiber, as these ceramics are known to improve mechanical toughness.[39] Electrospun PI mats have a much more frayed appearance compared to the higher PSSQ content fibers. Also, the other organic moiety present on the pristine PSSQ Si-O backbone is a nonpolar phenyl group, which is known to be fully removed at temperatures higher than those used in this study.[41] The minimal presence of this nonpolar group could introduce non-favorable electrolyte interactions with the separator.

Combined effects of superior electrolyte uptake and porosity lead to greater electrolyte ionic conductivities compared to Celgard for the electrospun separators. The addition of PSSQ causes an increase in average ionic conductivity for the 95/5 and 90/10 PI/PSSQ cases over PI only. Adding ceramic fillers into the fiber matrix has been previously shown to increase the overall amorphous content by preventing crystalline domain formation within the fiber during the fast-drying electrospinning

process, thus leading to improved ionic conductivity through these regions.[42] Additionally, ceramic inclusions in the polymer matrix can improve ion conduction through Lewis acid-base interactions of the terminal surface groups and electrolyte salts to increase salt dissociation.[43] Too much ceramic present in the fiber structure could present marginal benefit or even reduce conductivity due to the generally lower ionic conductivity of inorganics, as seen with the 80/20 PI/PSSQ separators.[44,45] The more aggregated ceramic domains formed through the high ceramic content potentially hinder ion transport through the fibers.[35] This, in conjunction with lower electrolyte uptake, decrease bulk ionic conductivity for the 80/20 PI/PSSQ separators.

Table 2.1 Comparison of separator properties

| Separator | Mean Pore Size (nm) | Electrolyte Uptake (%) | Ionic Conductivity (mS/cm) |
|---|---|---|---|
| **Celgard 2400** | ----- | 174 ± 16 | 0.56 |
| **PI Only** | 277 ± 157 | 1829 ± 48 | 1.98 ± 0.18 |
| **95/5 PI/PSSQ** | 225 ± 136 | 1426 ± 76 | 2.13 ± 0.05 |
| **90/10 PI/PSSQ** | 190 ± 142 | 1415 ± 75 | 2.17 ± 0.07 |
| **80/20 PI/PSSQ** | 232 ± 171 | 1377 ± 41 | 1.92 ± 0.09 |

Although PI has been shown to be thermally stable up to temperatures over 400 °C, for separator applications it is vital membrane does not shrink at elevated temperatures possibly encountered in battery operation. For this reason, the hybrid PI-based separators were subjected to a hot oven test at 150 °C for 2 hours, with Celgard included for comparison. Fig. 2.4a shows the pristine membranes before the test, whereas Fig. 2b shows the results afterwards. The initially 16 mm Celgard separator shrinks and becomes clear after exposure to the elevated temperature. By sharp contrast, all PI separators maintain their initial shape without any areal shrinkage. This

was to be expected as all PI separators are stable in the 300 °C heat treatment step after electrospinning. At elevated temperatures, there would be no issue of battery short-circuit with these PI and PI/PSSQ separators due to separator shrinkage and electrode contact.

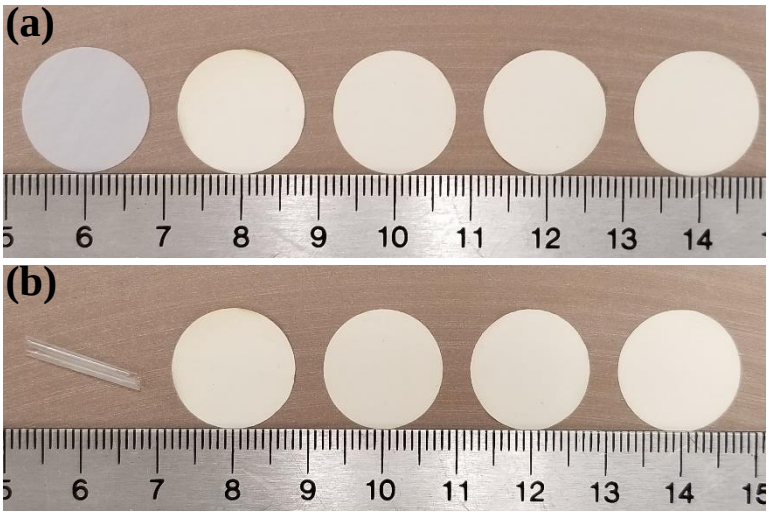


**Figure 2.4.** Dimensional thermal stability test of the hybrid separators at 150 °C for 2 hours. Separators from left to right: Celgard 2400, PI Only, 95/5 PI/PSSQ, 90/10 PI/PSSQ, 80/20 PI/PSSQ.

Polyimides are also known for their non-flammable properties. When exposed to high levels of heat and oxygen, a carbon char forms on the polyimide surface, protecting the bulk polymer layers and preventing further oxidation.[46] To test this, strips of Celgard 2400 and 90/10 PI/PSSQ were set aflame with a butane torch after soaking in excess electrolyte. Fig. 2.5a-b shows the pristine Celgard and 90/10 PI/PSSQ before being soaked with electrolyte. Fig. 2.5c shows the results of Celgard after the test, which had severely deformed. The polypropylene separator was not able to handle

intense heat and oxidation, thus completely losing its original dimensions. In stark contrast to Celgard, as shown in Fig. 2.5d, the PI/PSSQ composite non-woven separator showed good dimensional stability under such extreme conditions. A few bubbles formed on the membrane surface, but it was in otherwise good condition. Fig. 2.5e shows that the composite membrane was able to be handled with tweezers and had retained its original integrity. High heat tolerance and non-flammability of the polyimide were able to minimize the effect of harsh abuse conditions. In a battery system the good dimensional stability of these PI/PSSQ hybrid separators would prevent a short circuit from the electrodes contacting each other, even in the event of a fire. This could help minimize or isolate failure of individual battery cells at the pack level, preventing catastrophic failure of the entire system.

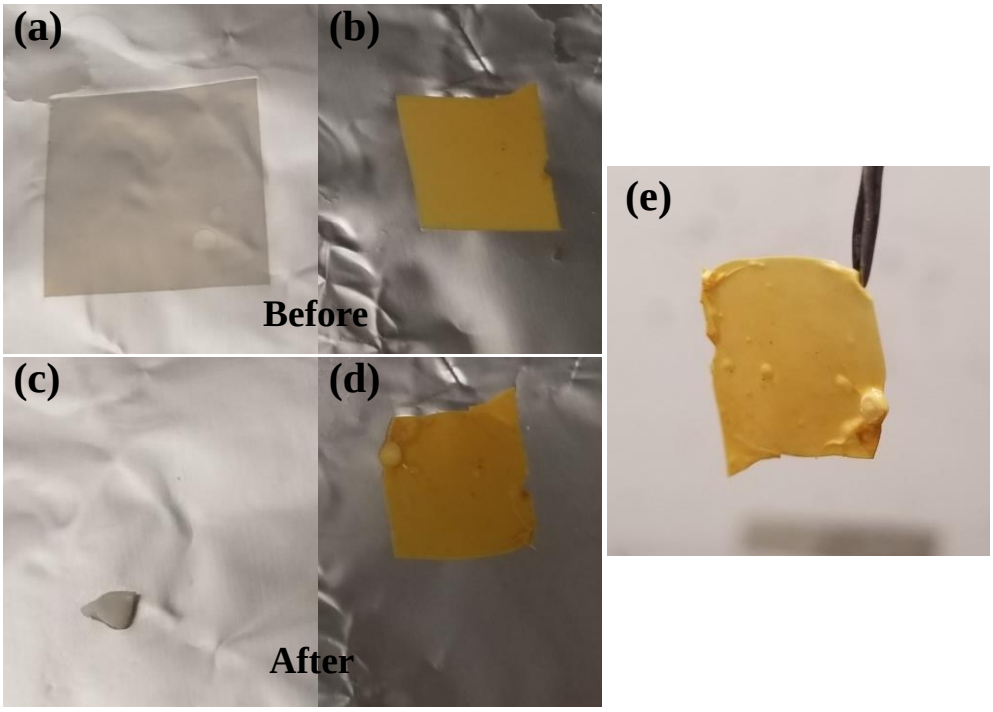


**Figure 2.5.** Flammability test of the separators. (a) and (b) are Celgard 2400 and 90/10 PI/PSSQ membranes before the test, respectively. (c) and (d) are the results of Celgard

2400 and 90/10 PI/PSSQ, respectively, after soaking with excess electrolyte and ignition with a butane torch. (e) 90/10 PI/PSSQ intact membrane after the test.

To be viable for use in lithium metal battery systems, the separator material must be stable against lithium in the voltage operating window. Electrochemical oxidation limits of Celgard, PI only, and 90/10 PI/PSSQ separators were investigated with linear sweep voltammetry as shown in Fig. 2.6. The electrochemical oxidation limit can be defined as the point where current sharply increases as the electrolyte breaks down. It is seen that the limit for all three separators falls around 4.6 V, with the PI and PI/PSSQ separators shifted closer to 4.7 V. This improvement is marginal but could be attributed to the better coordination of electrolyte with the more hydrophilic polyimide as opposed to the hydrophobic polypropylene Celgard. Also, the marginal improvement in stability of the PI/PSSQ separator over PI only can be explained by the Lewis acid-base interactions of electrolyte salts with the ceramic, further helping to delay oxidative decomposition.[47] Both PI and PI/PSSQ separators exhibited a slight increase in current beginning around 4.2 V. This can be attributed to reversible oxidation of the aromatic imide group.[48] However, all materials are clearly stable in the 1.8 to 2.8 V window used for Li-S cells in this study.

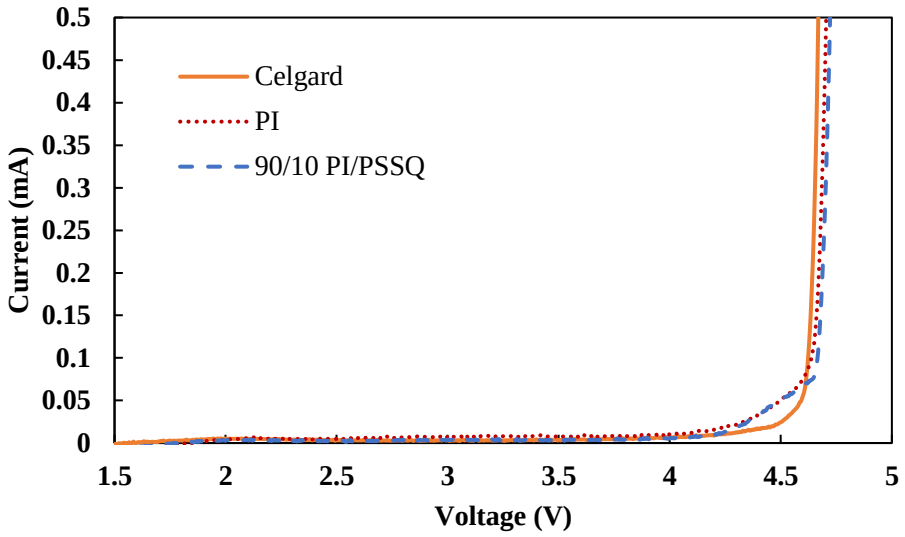


**Figure 2.6.** LSV of Celgard 2400, PI only, and 90/10 PI/PSSQ separators showing their stability against lithium metal.

The low rate 0.2C cycling performance for PI only and 95/5, 90/10, and 80/20 PI/PSSQ are shown in Fig. 2.7. Even though these separators have double the thickness (50 μm) compared to Celgard (25 μm), they achieve comparable performance at low rates due to the high ionic conductivities of the non-woven membranes. It should be noted that 50 μm is one of the smallest thicknesses reported for non-woven separators in Li-S research at this time. There is enough time for lithium ions to diffuse through all separators at these low rates. However, initial capacity does increase from 1092 mAh/g for Celgard to 1175, 1171, 1161, and 1164 mAh/g for PI and 95/5, 90/10, 80/20 PI/PSSQ separators, respectively.

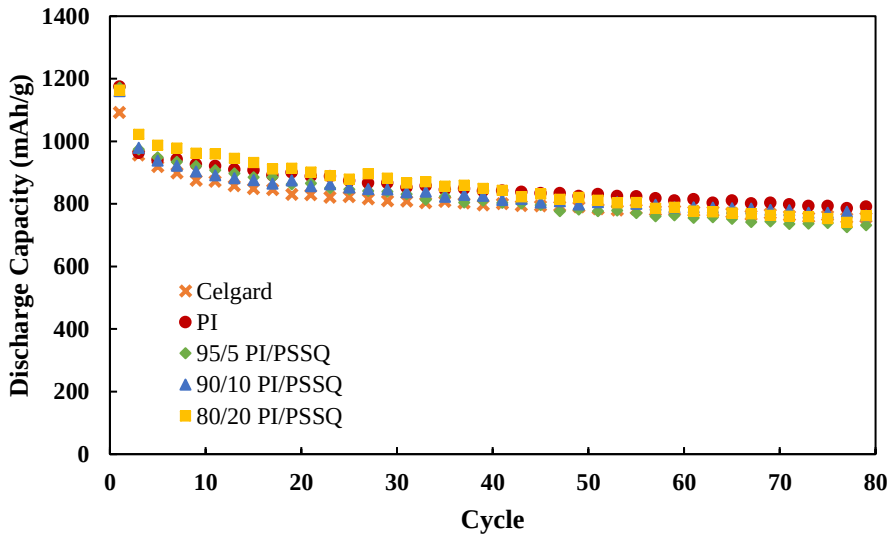


**Figure 2.7.** Cycling behavior for the various hybrid non-woven separators at 0.2C charge/discharge.

Differences in the initial discharge capacities can be explained by examining 0.2C 1st discharge profiles, shown in Fig. 2.8. For all hybrid non-woven separators, the onset of the lower voltage plateau is shifted towards higher capacities. This is due to improved sulfur utilization in the higher plateau region where more elemental sulfur can be reduced to higher order soluble lithium polysulfides.[49,50] High ion conduction in the non-woven membranes allows for any soluble sulfur or polysulfides that diffused away from the cathode to travel back during the discharge process more easily than through the narrow slit-like pores of Celgard. Generating more soluble polysulfides translated into longer low-voltage plateaus, as there is more $Li_2S_4$ to convert into insoluble $Li_2S$ species.

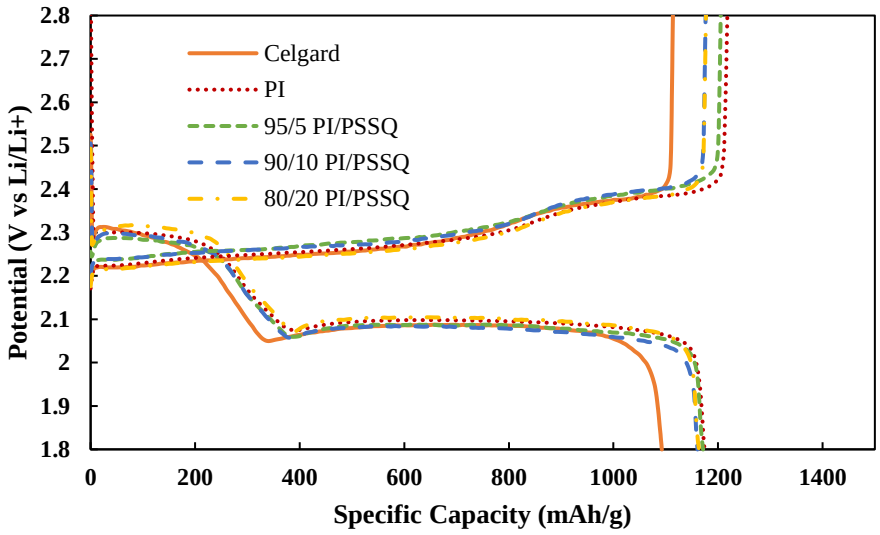


**Figure 2.8.** First galvanostatic discharge profiles at a current density of 0.2C.

High rate performance is essential for viable next-generation battery materials. For the sulfur cathode employed in this work, even Celgard provides sufficient ion diffusion even at high 1C charge/discharge rates, initially delivering 685 mAh/g compared to 717, 772, 712, and 708 mAh/g for PI only and 95/5, 90/10, and 80/20 PI/PSSQ separators, respectively. At harsher 2C charge/discharge conditions, the narrow channels of Celgard cannot deliver the necessary lithium ions to the cathode for proper sulfur reduction, and the difference between the separator types is unambiguous. At 2C, the initial discharge capacity for Celgard drops to a meager 214 mAh/g, whereas the PI and 95/5, 90/10, and 80/20 PI/PSSQ separators deliver 618, 683, 631, and 610 mAh/g, respectively. 95/5 PI/PSSQ outperforms the other hybrid separators at the harsher 0.5C, 1C, and 2C rates. This is likely due to a more optimum combination of ceramic content, fiber size, and fiber structure. The slightly smaller fibers and presence of more beads in the structure likely provide more surface area to influence

interactions between the separator and ions present in the electrolyte, with a more optimal dispersion of ceramic throughout the fibers. When returning to very mild 0.1C charge/discharge after the higher rates, all separators show an initially lower discharge capacity from the transition into a fast 2C charge to a slow 0.1C discharge due to limited active material being fully converted back into elemental sulfur and lithium metal during the fast charge. For the 2nd discharge of the 0.1C recovery cycles, Celgard provides a discharge capacity of 799 mAh/g. Cells with PI only and 95/5, 90/10 and 80/20 PI/PSSQ separators recover to 831, 899, 889, and 849 mAh/g in their 2nd 0.1C recovery cycles, respectively. These results show that the non-woven separators allow for reversible Li-S cell operation at higher cycling rates due to their ability to improve redox reaction kinetics with improved ion transport. Similar trends have been observed in glass fiber separators, due to their highly porous nature and electrolyte affinity not unlike the separators in this work.[26]

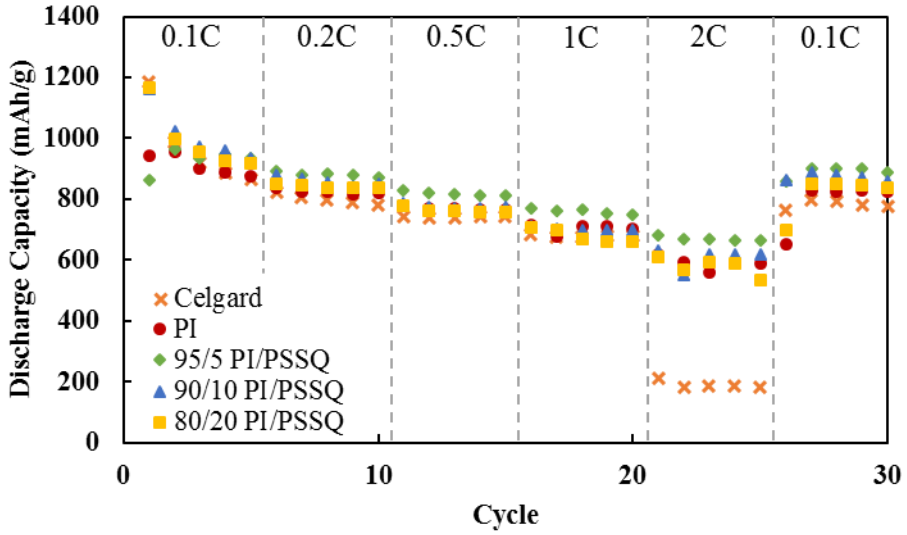


**Figure 2.9.** Rate capability performance at different current densities.

## 2.4 Conclusion

Polyimide/polysilsesquioxane hybrid separators were successfully fabricated using a gas-assisted electrospinning technique, with up to 20 wt% PSSQ in the fibers obtained. These highly porous, nanofiber membranes can uptake significant amounts of electrolyte, leading to roughly four times the ionic conductivity of conventional microporous Celgard separators. PI only and PI/PSSQ separators are thermally stable at 150 °C and can even maintain their structural integrity after being ignited. Meanwhile, Celgard readily shrinks when subjected to high temperatures are in the presence of a flame. Application of these separators in lithium-sulfur cells provided impressive discharge capacities between 600 to 700 mAh/g at harsh 2C cycling conditions, owing to their ability to efficiently transport lithium ions between electrodes. These separators provide a solid framework for use in Li-S systems, with traditional separator modifications such as an interlayer providing potential to improve these results even further.

## References


(1) Scrosati, B.; Garche, J. Lithium Batteries: Status, Prospects and Future. *Journal of Power Sources*. 2010, pp 2419–2430. https://doi.org/10.1016/j.jpowsour.2009.11.048.

(2) Noorden, R. Van. Sulphur Back in Vogue for Batteries. *Nature* **2013**, *498* (7455), 416–417.

(3) Manthiram, A.; Fu, Y.; Su, Y. S. Challenges and Prospects of Lithium-Sulfur Batteries. *Acc. Chem. Res.* **2013**, *46* (5), 1125–1134. https://doi.org/10.1021/ar300179v.

(4) Bruce, P. G.; Freunberger, S. A.; Hardwick, L. J.; Tarascon, J. M. Li-O2 and Li-S Batteries with High Energy Storage. *Nat. Mater.* **2012**, *11* (1), 19–29. https://doi.org/10.1038/nmat3191.

(5) Larcher, D.; Tarascon, J. M. Towards Greener and More Sustainable Batteries for Electrical Energy Storage. *Nature Chemistry*. 2015, pp 19–29. https://doi.org/10.1038/nchem.2085.

(6) Zhang, X. Q.; He, B.; Li, W. C.; Lu, A. H. Hollow Carbon Nanofibers with Dynamic Adjustable Pore Sizes and Closed Ends as Hosts for High-Rate Lithium-Sulfur Battery Cathodes. *Nano Res.* **2018**, *11* (3), 1238–1246. https://doi.org/10.1007/s12274-017-1737-6.

(7) Zheng, G.; Yang, Y.; Cha, J. J.; Hong, S. S.; Cui, Y. Hollow Carbon Nanofiber-Encapsulated Sulfur Cathodes for High Specific Capacity Rechargeable Lithium Batteries. *Nano Lett.* **2011**, *11* (10), 4462–4467. https://doi.org/10.1021/nl2027684.

(8) Lee, J.; Ko, B.; Kang, J.; Chung, Y.; Kim, Y.; Halim, W.; Lee, J. H.; Joo, Y. L. Facile and Scalable Fabrication of Highly Loaded Sulfur Cathodes and Lithium–Sulfur Pouch Cells via Air-Controlled Electrospray. *Mater. Today Energy* **2017**, *6*, 255–263. https://doi.org/10.1016/j.mtener.2017.11.003.

(9) Gueon, D.; Hwang, J. T.; Yang, S. B.; Cho, E.; Sohn, K.; Yang, D. K.; Moon, J. H. Spherical Macroporous Carbon Nanotube Particles with Ultrahigh Sulfur Loading for Lithium-Sulfur Battery Cathodes. *ACS Nano* **2018**, *12* (1), 226–233. https://doi.org/10.1021/acsnano.7b05869.

(10) Dörfler, S.; Hagen, M.; Althues, H.; Tübke, J.; Kaskel, S.; Hoffmann, M. J. High Capacity Vertical Aligned Carbon Nanotube/Sulfur Composite Cathodes for Lithium-Sulfur Batteries. *Chem. Commun.* **2012**, *48* (34), 4097–4099. https://doi.org/10.1039/c2cc17925c.

(11) Su, Y. S.; Manthiram, A. A New Approach to Improve Cycle Performance of Rechargeable Lithium-Sulfur Batteries by Inserting a Free-Standing MWCNT Interlayer. *Chem. Commun.* **2012**, *48* (70), 8817–8819. https://doi.org/10.1039/c2cc33945e.

(12) Guo, J.; Xu, Y.; Wang, C. Sulfur-Impregnated Disordered Carbon Nanotubes Cathode for Lithium-Sulfur Batteries. *Nano Lett.* **2011**, *11* (10), 4288–4294. https://doi.org/10.1021/nl202297p.

(13) Ji, X.; Lee, K. T.; Nazar, L. F. A Highly Ordered Nanostructured Carbon-

Sulphur Cathode for Lithium-Sulphur Batteries. *Nat. Mater.* **2009**, *8* (6), 500–506. https://doi.org/10.1038/nmat2460.

(14) Schuster, J.; He, G.; Mandlmeier, B.; Yim, T.; Lee, K. T.; Bein, T.; Nazar, L. F. Spherical Ordered Mesoporous Carbon Nanoparticles with High Porosity for Lithium-Sulfur Batteries. *Angew. Chemie - Int. Ed.* **2012**, *51* (15), 3591–3595. https://doi.org/10.1002/anie.201107817.

(15) Song, J.; Xu, T.; Gordin, M. L.; Zhu, P.; Lv, D.; Jiang, Y. B.; Chen, Y.; Duan, Y.; Wang, D. Nitrogen-Doped Mesoporous Carbon Promoted Chemical Adsorption of Sulfur and Fabrication of High-Areal-Capacity Sulfur Cathode with Exceptional Cycling Stability for Lithium-Sulfur Batteries. *Adv. Funct. Mater.* **2014**, *24* (9), 1243–1250. https://doi.org/10.1002/adfm.201302631.

(16) Ji, L.; Rao, M.; Zheng, H.; Zhang, L.; Li, Y.; Duan, W.; Guo, J.; Cairns, E. J.; Zhang, Y. Graphene Oxide as a Sulfur Immobilizer in High Performance Lithium/Sulfur Cells. *J. Am. Chem. Soc.* **2011**, *133* (46), 18522–18525. https://doi.org/10.1021/ja206955k.

(17) Zhang, L.; Ji, L.; Glans, P. A.; Zhang, Y.; Zhu, J.; Guo, J. Electronic Structure and Chemical Bonding of a Graphene Oxide-Sulfur Nanocomposite for Use in Superior Performance Lithium-Sulfur Cells. *Phys. Chem. Chem. Phys.* **2012**, *14* (39), 13670–13675. https://doi.org/10.1039/c2cp42866k.

(18) Wang, H.; Yang, Y.; Liang, Y.; Robinson, J. T.; Li, Y.; Jackson, A.; Cui, Y.; Dai, H. Graphene-Wrapped Sulfur Particles as a Rechargeable Lithium-Sulfur Battery Cathode Material with High Capacity and Cycling Stability. *Nano Lett.* **2011**, *11* (7), 2644–2647. https://doi.org/10.1021/nl200658a.

(19) Chen, K.; Cao, J.; Lu, Q.; Wang, Q.; Yao, M.; Han, M.; Niu, Z.; Chen, J. Sulfur Nanoparticles Encapsulated in Reduced Graphene Oxide Nanotubes for Flexible Lithium-Sulfur Batteries. *Nano Res.* **2018**, *11* (3), 1345–1357. https://doi.org/10.1007/s12274-017-1749-2.

(20) Huang, J. Q.; Zhang, Q.; Wei, F. Multi-Functional Separator/Interlayer System for High-Stable Lithium-Sulfur Batteries: Progress and Prospects. *Energy Storage Mater.* **2015**, *1*, 127–145. https://doi.org/10.1016/j.ensm.2015.09.008.

(21) Su, Y. S.; Manthiram, A. Lithium-Sulphur Batteries with a Microporous Carbon Paper as a Bifunctional Interlayer. *Nat. Commun.* **2012**, *3*, 1166. https://doi.org/10.1038/ncomms2163.

(22) Rana, M.; Li, M.; Huang, X.; Luo, B.; Gentle, I.; Knibbe, R. Recent Advances in Separators to Mitigate Technical Challenges Associated with Re-Chargeable Lithium Sulfur Batteries. *J. Mater. Chem. A* **2019**, *7* (12), 6596–6615. https://doi.org/10.1039/c8ta12066h.

(23) Arora, P.; Zhang, Z. Battery Separators. *Chem. Rev.* **2004**, *104* (10), 4419–4462. https://doi.org/10.1021/cr020738u.

(24) Love, C. T. Thermomechanical Analysis and Durability of Commercial Micro-Porous Polymer Li-Ion Battery Separators. *J. Power Sources* **2011**, *196* (5), 2905–2912. https://doi.org/10.1016/j.jpowsour.2010.10.083.

(25) Song, J.; Ryou, M. H.; Son, B.; Lee, J. N.; Lee, D. J.; Lee, Y. M.; Choi, J. W.; Park, J. K. Co-Polyimide-Coated Polyethylene Separators for Enhanced

Thermal Stability of Lithium Ion Batteries. *Electrochim. Acta* **2012**, *85*, 524–530. https://doi.org/10.1016/j.electacta.2012.06.078.

(26) Zhu, J.; Yanilmaz, M.; Fu, K.; Chen, C.; Lu, Y.; Ge, Y.; Kim, D.; Zhang, X. Understanding Glass Fiber Membrane Used as a Novel Separator for Lithium-Sulfur Batteries. *J. Memb. Sci.* **2016**, *504*, 89–96. https://doi.org/10.1016/j.memsci.2016.01.020.

(27) Zhu, J.; Ge, Y.; Kim, D.; Lu, Y.; Chen, C. A Novel Separator Coated by Carbon for Achieving Exceptional High Performance Lithium-Sulfur Batteries. *Nano Energy* **2016**, *20*, 176–184. https://doi.org/10.1016/j.nanoen.2015.12.022.

(28) Li, Y.; Zhu, J.; Zhu, P.; Yan, C.; Jia, H.; Kiyak, Y.; Zang, J.; He, J.; Dirican, M.; Zhang, X. Glass Fiber Separator Coated by Porous Carbon Nanofiber Derived from Immiscible PAN/PMMA for High-Performance Lithium-Sulfur Batteries. *J. Memb. Sci.* **2018**, *552*, 31–42. https://doi.org/10.1016/j.memsci.2018.01.062.

(29) Zhu, J.; Chen, C.; Lu, Y.; Zang, J.; Jiang, M.; Kim, D.; Zhang, X. Highly Porous Polyacrylonitrile/Graphene Oxide Membrane Separator Exhibiting Excellent Anti-Self-Discharge Feature for High-Performance Lithium-Sulfur Batteries. *Carbon N. Y.* **2016**, *101*, 272–280. https://doi.org/10.1016/j.carbon.2016.02.007.

(30) Jeong, H. S.; Hong, S. C.; Lee, S. Y. Effect of Microporous Structure on Thermal Shrinkage and Electrochemical Performance of Al2O3/Poly(Vinylidene Fluoride-Hexafluoropropylene) Composite Separators for Lithium-Ion Batteries. *J. Memb. Sci.* **2010**, *364*, 177–182. https://doi.org/10.1016/j.memsci.2010.08.012.

(31) Liu, H.; Xu, J.; Guo, B.; He, X. Effect of Al2O3/SiO2 Composite Ceramic Layers on Performance of Polypropylene Separator for Lithium-Ion Batteries. *Ceram. Int.* **2014**, *40*, 14105–14110. https://doi.org/10.1016/j.ceramint.2014.05.142.

(32) Raghavan, P.; Zhao, X.; Manuel, J.; Chauhan, G. S.; Ahn, J. H.; Ryu, H. S.; Ahn, H. J.; Kim, K. W.; Nah, C. Electrochemical Performance of Electrospun Poly(Vinylidene Fluoride-Co-Hexafluoropropylene)-Based Nanocomposite Polymer Electrolytes Incorporating Ceramic Fillers and Room Temperature Ionic Liquid. *Electrochim. Acta* **2010**, *55* (4), 1347–1354. https://doi.org/10.1016/j.electacta.2009.05.025.

(33) Wang, Y.; Wang, S.; Fang, J.; Ding, L. X.; Wang, H. A Nano-Silica Modified Polyimide Nanofiber Separator with Enhanced Thermal and Wetting Properties for High Safety Lithium-Ion Batteries. *J. Memb. Sci.* **2017**, *537* (January), 248–254. https://doi.org/10.1016/j.memsci.2017.05.023.

(34) Yanilmaz, M.; Lu, Y.; Zhu, J.; Zhang, X. Silica/Polyacrylonitrile Hybrid Nanofiber Membrane Separators via Sol-Gel and Electrospinning Techniques for Lithium-Ion Batteries. *J. Power Sources* **2016**, *313*, 205–212. https://doi.org/10.1016/j.jpowsour.2016.02.089.

(35) Smith, S. A.; Park, J. H.; Williams, B. P.; Joo, Y. L. Polymer/Ceramic Co-Continuous Nanofiber Membranes via Room-Curable Organopolysilazane for

Improved Lithium-Ion Battery Performance. *J. Mater. Sci.* **2017**, *52* (7), 3657–3669. https://doi.org/10.1007/s10853-016-0574-4.

(36) Smith, S. A.; Williams, B. P.; Joo, Y. L. Effect of Polymer and Ceramic Morphology on the Material and Electrochemical Properties of Electrospun PAN/Polymer Derived Ceramic Composite Nanofiber Membranes for Lithium Ion Battery Separators. *J. Memb. Sci.* **2017**, *526* (December 2016), 315–322. https://doi.org/10.1016/j.memsci.2016.12.052.

(37) Liaw, D.-J.; Chang, F.-C.; Leung, M.; Chou, M.; Muellen, K. High Thermal Stability and Rigid Rod of Novel Organosoluble Polyimides and Polyamides Based on Bulky and Noncoplanar Naphthalene−Biphenyldiamine. *Macromolecules* **2005**, *38* (9), 4024–4029. https://doi.org/10.1021/ma048559x.

(38) Choi, S. S.; Lee, A. S.; Lee, H. S.; Jeon, H. Y.; Baek, K. Y.; Choi, D. H.; Hwang, S. S. Synthesis and Characterization of UV-Curable Ladder-like Polysilsesquioxane. *J. Polym. Sci. Part A Polym. Chem.* **2011**, *49* (23), 5012–5018. https://doi.org/10.1002/pola.24942.

(39) Kim, Y. H.; Choi, G. M.; Bae, J. G.; Kim, Y. H.; Bae, B. S. High-Performance and Simply-Synthesized Ladder-like Structured Methacrylate Siloxane Hybrid Material for Flexible Hard Coating. *Polymers (Basel).* **2018**, *10* (4). https://doi.org/10.3390/polym10040449.

(40) Lee, K. H.; Kim, H. Y.; Bang, H. J.; Jung, Y. H.; Lee, S. G. The Change of Bead Morphology Formed on Electrospun Polystyrene Fibers. *Polymer (Guildf).* **2003**, *44* (14), 4029–4034. https://doi.org/10.1016/S0032-3861(03)00345-8.

(41) Wang, J.; He, C.; Lin, Y.; Chung, T. S. Studies on the Thermal Stability of F- and Non-F-Containing Ladder Polyepoxysilsesquioxanes by TGA-FTIR. *Thermochim. Acta* **2002**, *381* (1), 83–92. https://doi.org/10.1016/S0040-6031(01)00644-X.

(42) Angulakshmi, N.; Nahm, K. S.; Swaminathan, V.; Thomas, S.; Nimma Elizabeth, R. Nanocomposite Polymer Electrolytes for Lithium Batteries. In *Polymer Processing and Characterization*; 2012; Vol. 394, pp 55–65. https://doi.org/10.1201/b13105.

(43) Plichta, E.; Greenbaum, S. G.; Scrosati, B.; Chung, S. H.; Wang, Y.; Croce, F.; Persi, L. Enhancement of Ion Transport in Polymer Electrolytes by Addition of Nanoscale Inorganic Oxides. *J. Power Sources* **2002**, *97–98*, 644–648. https://doi.org/10.1016/s0378-7753(01)00748-0.

(44) Raghavan, P.; Choi, J. W.; Ahn, J. H.; Cheruvally, G.; Chauhan, G. S.; Ahn, H. J.; Nah, C. Novel Electrospun Poly(Vinylidene Fluoride-Co-Hexafluoropropylene)-in Situ SiO2 Composite Membrane-Based Polymer Electrolyte for Lithium Batteries. In *Journal of Power Sources*; 2008; Vol. 184, pp 437–443. https://doi.org/10.1016/j.jpowsour.2008.03.027.

(45) Knauth, P. Inorganic Solid Li Ion Conductors: An Overview. *Solid State Ionics* **2009**, *180* (14–16), 911–916. https://doi.org/10.1016/j.ssi.2009.03.022.

(46) Morgan, A. B.; Putthanarat, S. Use of Inorganic Materials to Enhance Thermal Stability and Flammability Behavior of a Polyimide. *Polym. Degrad. Stab.*

**2011**, *96* (1), 23–32. https://doi.org/10.1016/j.polymdegradstab.2010.11.005.

(47) Lee, J. Y.; Lee, Y. M.; Bhattacharya, B.; Nho, Y. C.; Park, J. K. Separator Grafted with Siloxane by Electron Beam Irradiation for Lithium Secondary Batteries. *Electrochim. Acta* **2009**, *54* (18), 4312–4315. https://doi.org/10.1016/j.electacta.2009.02.088.

(48) Song, Z.; Zhan, H.; Zhou, Y. Polyimides: Promising Energy-Storage Materials. *Angew. Chemie - Int. Ed.* **2010**, *49* (45), 8444–8448. https://doi.org/10.1002/anie.201002439.

(49) Bruce, P. G.; Freunberger, S. A.; Hardwick, L. J.; Tarascon, J. M. Li-O2 and Li-S Batteries with High Energy Storage. *Nature Materials*. December 15, 2012, pp 19–29. https://doi.org/10.1038/nmat3191.

(50) Ellis, B. L.; Lee, K. T.; Nazar, L. F. Positive Electrode Materials for Li-Ion and Li-Batteries. *Chem. Mater.* **2010**, *22* (3), 691–714. https://doi.org/10.1021/cm902696j.

# Chapter 3. Reduced Graphene Oxide Interlayer for Polyimide/Ceramic Composite Non-Woven Separators in Lithium-Sulfur Batteries

## 3.1 Introduction

Batteries that can provide greater specific energy and energy density than current lithium ion chemistry are needed for next generation electric vehicles, grid storage, and personal electronics.[1–3] Lithium-sulfur (Li-S) has been intensely studied to fill this role as it boasts a high theoretical specific capacity of 1675 mAh/g and energy density of 2600 Wh/kg.[4,5] Furthermore, elemental sulfur is nontoxic, naturally abundant, and inexpensive.[3] Unlike the intercalation cathodes of lithium-ion, sulfur is converted to lithium polysulfides through a series of reactions, providing the high capacity and energy output. However, there are several challenges with Li-S preventing its full commercialization.

One of the main issues is that sulfur and the final $Li_2S$ discharge product are electrically insulating, so a conductive framework is necessary to improve utilization of the active material. Another main challenge is that higher order lithium polysulfides ($Li_2S_X$, $4 \leq X \leq 8$) are soluble in typical organic electrolytes and tend to diffuse or "shuttle" to the lithium metal anode and react, causing significant capacity fading as the battery cycles.[5–7] One way to mitigate these issues that has been heavily investigated is to use nanostructured carbon host materials for sulfur, forming carbon-sulfur composites.[8,9] Carbon nanotubes,[10–12] graphene oxide,[13,14] reduced graphene oxide,[15,16] porous carbon particles,[9,17] and carbon nanofibers[18,19] have all been used as

sulfur host materials to improve active material utilization and help trap soluble polysulfides in the cathode region.

An additional layer between the cathode and separator, known as an interlayer, has been introduced to help mitigate the polysulfide shuttling issue.[5,20,21] This layer operates by acting as a physical barrier and/or trapping polysulfides with physical or chemical means. Conductive interlayers also can act as a "second current collector" to further reduce any polysulfides that get trapped in the layer, as illustrated with the pioneering carbon interlayer, a microporous carbon paper.[20] Various carbons have been also been investigated for this purpose, such as carbon nanotubes,[22] carbon nanofibers,[23] graphene,[24,25] and mesoporous carbons.[26] Carbons functionalized with nitrogen[27] or sulfonate[28] groups have the additional ability to trap polysulfides through chemisorption. Ion conducting polymers such as Nafion[29,30] or PEDOT:PSS[31] also function in this way but need to be mixed with an electronically conductive material to reactivate any trapped polysulfides.

In this work, the previously developed thermally stable and high-rate performing polyimide (PI)/polysilsesquioxane (PSSQ) separators serve as the basis for additional separator modifications to improve lithium-sulfur battery performance even further. Reduced graphene oxide is applied as an interlayer via a facile air-controlled electrospraying technique and serves as a physical barrier for polysulfide diffusion while acting as an upper current collector and improving overall ionic conductivity of the membranes. This in turn leads to lowered charge-transfer resistance in Li-S cells and improves battery performance even at lower charge/discharge rates.

## 3.2 Experimental Methods

### 3.2.1 Preparation of Polyimide/Ceramic Non-Woven Separators via Gas-Assisted Electrospinning

All materials used in this study were purchased from Sigma-Aldrich unless otherwise stated. Polyimide/ceramic hybrid separators were prepared using the gas-assisted electrospinning method. P84 polyimide (Powder, Evonik) was dissolved in N,N-dimethylformamide (DMF) to form a 16 wt% solution, and stirred on a 65 °C hotplate overnight. The ladder polysilsesquioxane (PSSQ) ceramic used was PMK (DJ Semichem). One hour prior to electrospinning, the solution was removed from the hot plate and PMK was added such that it was 10 wt% of the total solid content. The solution was then stirred at room temperature until the PMK was thoroughly dissolved, and vigorously stirred on a vortex mixer for two minutes to ensure a homogeneous mixture before electrospinning. A Harvard Apparatus PHD Ultra was used to electrospin the solution onto an aluminum foil current collector in a chamber controlled at 16 % relative humidity. A coaxial needle with 12-gauge inner needle and 16-gauge outer shell was used. The solution was fed through the inner needle at an infusion rate of 0.03 mL/min, and 16 % RH dry air was supplied through the outer shell at an air pressure of 10 psi. The tip-to-collector distance and applied voltage were 15 cm and 25 kV, respectively. The resulting fiber mat was peeled from the collector and heat treated at 300 °C under air for 3 hours with a 5 °C/min ramp rate. The fiber mat was then punched into 16 mm diameter discs and cold-calendered to about 50 μm in thickness before use.

### 3.2.2 Reduced Graphene Oxide (rGO) Coated Separators via Air-Controlled Electrospraying

Both Celgard and PI/PSSQ were coated with reduced graphene oxide (rGO) using an air-controlled electrospraying method with the same experimental setup as for gas-assisted electrospinning above. Coated Celgard and PI/PSSQ are referred to as rGO-Celgard and rGO-PI/PSSQ, respectively. To prepare the rGO dispersion for electrospraying, a 6 wt% dispersion of rGO in water (ACS Materials) was diluted to 4 wt% with distilled water. This solution was placed in a bath sonicator for 30 minutes prior to electrospraying to ensure a homogeneous dispersion. A solution flow rate of 0.05 mL/min was fed through the inner tip of the coaxial nozzle, while 16 % RH dry air was supplied to the outer shell with an air pressure of 15 psi. The applied voltage was set to 25 kV, and the tip-to-collector distance was 15 cm. The Celgard and PI/PSSQ separators were held onto the aluminum foil collector only through static forces and the uniaxial air flow. The mass loading of the graphene coatings was kept between 0.25 to 0.3 mg/cm$^2$.

### 3.2.3 Material Characterization

To study the morphology of the electrosprayed rGO coating, field emission scanning electron microscopy (FESEM, Tescan Mira3) with an accelerating voltage of 5 kV was employed.

### 3.2.4 Electrochemical Characterization

The electrolyte consisted of 1 M lithium bis(trifluoromethane) sulfonimide (LiTFSI) and 1 wt% lithium nitrate ($LiNO_3$) in a 1:1 volume mixture of 1,3-dioxolane (DOL) and 1,2-dimethoxyethane (DME). Electrolyte uptake was determined by soaking the separators in electrolyte for two hours, and calculating the mass change with the equation:

$$Electrolyte\ Uptake\ (\%) = \frac{W_f - W_i}{W_i}\ x\ 100 \qquad (2)$$

Where $W_i$ and $W_f$ are the masses of the separator before and after soaking in liquid electrolyte for two hours, respectively.

Ionic conductivity was measured using electrochemical impedance spectroscopy (EIS, Parstat 4000, Princeton Applied Materials). For these tests, un-coated and coated separators were soaked with 25 and 45 µL of electrolyte, respectively, to mimic battery cell conditions. They were then sandwiched between two stainless steel discs in a CR2032 coin cell. A frequency range from 100 kHz to 0.1 Hz was applied with an AC amplitude of 10 mV. Ionic conductivity was calculated according to the equation:

$$\sigma = \frac{d}{R_b\ x\ A} \qquad (3)$$

Where d is the thickness of the separator, $R_b$ is the bulk resistance, and A is the surface area of the stainless steel electrode (1.96 $cm^2$). $R_b$ is defined as the high frequency intercept of the real axis.

CR2032 coin cells were assembled to tests the electrochemical performance of the polyimide/ceramic separators in Li-S. The slurry cathode used in this study was prepared by first infiltrating sulfur into porous carbons. Active sulfur material

(Spectrum Chemical) was mixed with Ketjenblack (KB, EC-600JD, AkzoNobel) at a 3:1 ratio, then grinded and heated at 155 °C for 12 hours in a hydrothermal reactor to melt impregnate the sulfur into the KB. Polyvinylidene fluoride (PVDF) was dissolved in N-methyl-2-pyrrolidone (NMP) at 10 wt% to serve as the binder. Super C65 (TIMCAL) was used as the conductive carbon. A homogeneous slurry was formed by combining NMP with 70 wt% S/KB, 20 wt% Super C65 and 10 wt% PVDF and mixing for 3 hours in a ball mixer. This was then cast onto aluminum foil with a doctor blade. The slurry was dried at 60 °C under vacuum for 12 hours and punched into 15 mm discs. The mass loading of active sulfur material was between 0.95 to 1.1 $mg/cm^2$. Li-S coin cells were fabricating by placing the separator between the slurry cathode and lithium metal foil. Celgard 2400 was used as the reference separator in this work. An electrolyte ratio of 15 μL/mg S was added to the uncoated separators, whereas 25 and 20 μL/mg S were added to rGO-Celgard and rGO-PI/PSSQ, respectively. Coin cells were cycled between 1.8 and 2.8 V vs $Li/Li^+$ using a Landt battery tester. All discharge capacities and current densities are based on active sulfur mass. Current densities were set according to a sulfur theoretical specific capacity of 1675 mAh/g. EIS of Li-S cells was completed using the Parstat 4000 in the frequency range 100 kHz to 10 mHz with a 10mV AC amplitude.

## 3.3 Results and Discussion

Air-controlled (AC) electrospraying provides a facile means to deposit uniform coating layers on the surface of substrates. The addition of the coaxial air jet to conventional electrospraying helps to break apart the solution jet into even smaller

droplets, which deposit in a smooth and uniform layer. This has the added benefit over typical dip-coating, vacuum filtration, or slurry casting methods that the drying step after deposition is eliminated. Fig. 3.1a shows Celgard before and after being coated by rGO. A smooth, uniform gray film was deposited onto its surface, with no visible signs of cracks or deformities. Fig. 3.1b similarly shows PI/PSSQ separators both with and without the AC electrosprayed rGO coating. The rGO layer on PI/PSSQ separators appear to have a darker hue, likely do the rougher surface of the non-woven polymer/ceramic separators from their porous and fibrous nature. The coating also appears to take the shape of any defects/nonuniformities on the surface. Since Celgard is a polypropylene film, it has a uniformly even surface for smooth deposition.

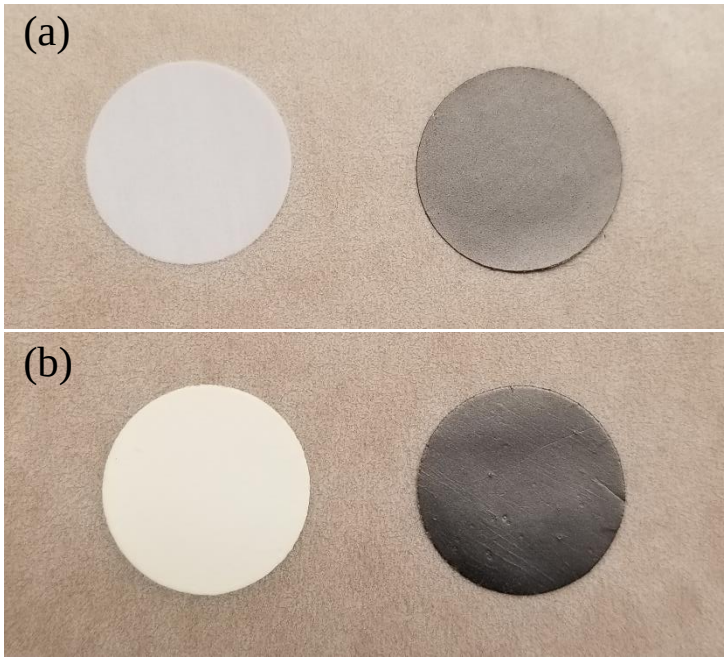


**Figure 3.1.** Digital photographs of (a) pristine (left) and rGO-coated (right) Celgard, and (b) pristine (left) and rGO-coated (right) PI/PSSQ.

This is further confirmed by analyzing the coatings at high magnifications. Fig. 3.2a and b show the rGO layers on Celgard and PI/PSSQ, respectively. Fig. 3.2a shows that the Celgard coating is very dense, which makes it more susceptible to cracking. On the other hand, the layer on PI/PSSQ has a more loosely packed structure, as the fibrous surface prevents close packing of the rGO sheets. This helps to explain the color difference between the separators observed at the macroscale. An analogous result has been observed for the difference in electrospraying vs. slurry casting Li-S cathodes.[32] Due to the dense layer formed by conventional slurry casting cathode materials, they are susceptible to crack formation during drying and processing steps. However, the electrospraying method deposits a dry and more porous cathode structure on the current collector, preventing this crack formation altogether.

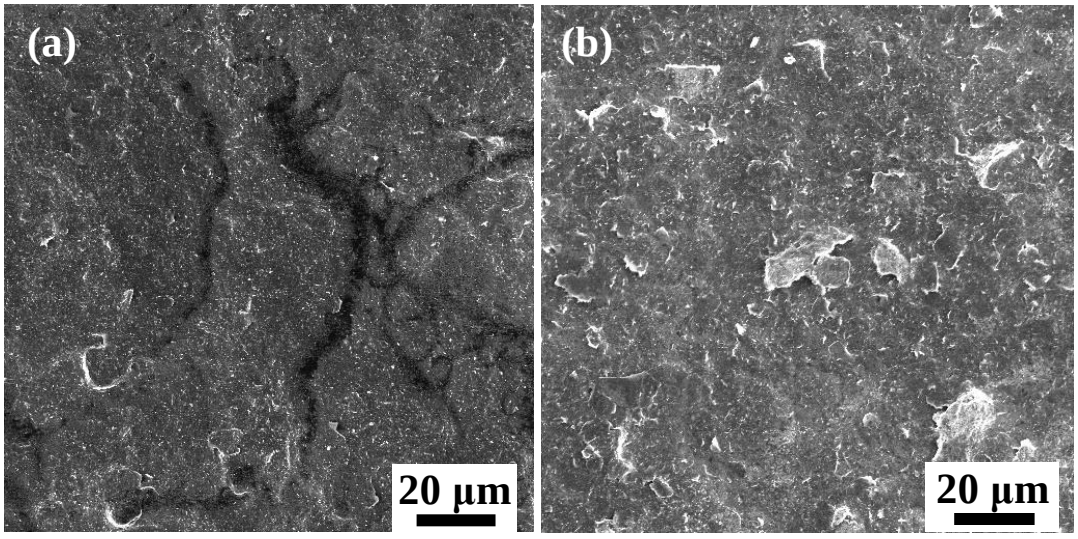


**Figure 3.2.** Top-view SEM images of (a) rGO-Celgard and (b) rGO-PI/PSSQ.

As discussed in the previous chapter, PI/PSSQ membranes are able to uptake significantly higher amounts of battery electrolyte than microporous Celgard due to their highly porous fiber structure and more hydrophilic materials. The effect of rGO coatings on the ability of separators to uptake electrolyte was investigated, with results presented in Table 3.1. For the Celgard case, the additional rGO serves to improve the amount of electrolyte the separator can hold as it serves as an added reservoir to hold the liquid. However, for the non-woven separator the addition of the layer decreases the amount of electrolyte that could be held in the membrane. There are two possible explanations for this. The first is that by adding rGO to the surface, the membrane becomes more rigid. This impedes expansion of the fibrous structure to accommodate a higher volume of liquid in the pore space, thus lowering the total amount of liquid the membrane can hold. The second explanation is that during the electrospraying process, rGO sheets partially penetrate the pores between fibers rather than just staying on the surface such as for Celgard, and essentially reduce the total pore volume. This would then lower total electrolyte uptake as the membrane porosity is decreased and the additional rGO layer cannot accommodate as much liquid as the non-woven membrane.

Coating the separators with rGO also has a significant effect on their ionic conductivity. In both cases, the additional layer improves ion transport through the membrane. For Celgard, the improvement can be attributed to increased electrolyte retention in the membrane, allowing more ions present for transport.[33] The case for PI/PSSQ separators is harder to explain, as the drop in electrolyte uptake does not appear to reduce the overall ionic conductivity of the membrane. The more porous

rGO layer potentially allows easy transport of ions than the dense layer formed on Celgard. A rigid rGO layer limits swelling of the non-woven membrane in the presence of liquid electrolyte, improving the coordination of electrolyte solvent and salts with the nanofibers.

Table 3.1. Comparison of separator properties

| Separator | Electrolyte Uptake (%) | Ionic Conductivity (mS/cm) |
|---|---|---|
| **Celgard** | 152 ± 35 | 0.49 |
| **rGO-Celgard** | 182 ± 48 | 0.82 ± 0.05 |
| **PI/PSSQ** | 1345 ± 52 | 1.74 ± 0.04 |
| **rGO-PI/PSSQ** | 962 ± 52 | 2.19 ± 0.10 |

Electrochemical impedance spectroscopy was also used to analyze the effects on resistance of the added rGO, as shown in Fig. 3.3. For both separators, the additional layer increases the high frequency resistance from the bulk electrolyte, since it must pass through an additional layer to reach the cathode.[31] This resistance was lower for both PI/PSSQ separators than the Celgard ones due to their higher ionic conductivities and more open, porous structure. rGO coating also lowered the charge-transfer resistances of the cells for both types of separators because it essentially acts as a second current collector and improves electrical conductivity at the cathode/separator interface, thus providing more electron pathways to active sulfur.[20] The positively sloped tail in the low-frequency region is known as Warburg diffusion, which indicates the diffusion of lithium ions and polysulfides at the cathode.[34] For both PI/PSSQ cells the slope of this region is higher than that of either Celgard cells, indicating sulfur reactions are less kinetically limited with the non-woven separators.

This should translate into improved performance compared to Celgard at higher charge/discharge rates, where overall reaction kinetics are critical.

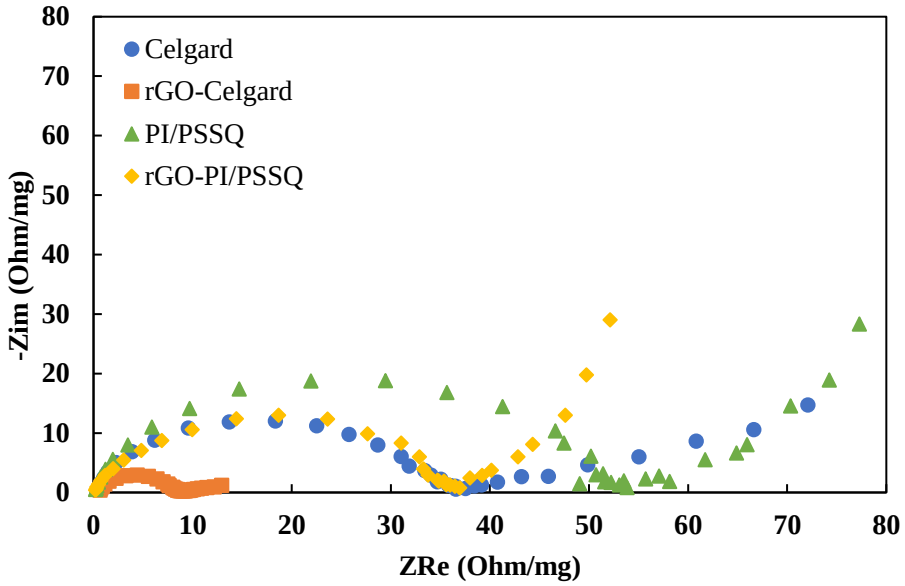


**Figure 3.3.** Electrochemical impedance spectra of Li-S cells with the different separators.

Cycling performance at different current densities for the various separators is presented in Fig. 3.4. rGO-Celgard shows higher discharge capacities than pristine Celgard at all rates but 2C, owing to improved ionic conductivity and the ability of rGO to provide additional reaction sites for polysulfides by acting as an upper current collector. At harsh 2C charge/discharge conditions, the poor performance of the base microporous separator limits the improvement a conductive carbon interlayer can provide. Fast ion transport through PI/PSSQ separators results in far superior 2C cyclability, offering an improved base separator to use for interlayer coatings. rGO-PI/PSSQ similarly shows higher discharge capacity at rates from 0.1 to 1C compared

to pristine PI/PSSQ due to enhanced ionic conductivity and the ability to limit polysulfide diffusion into the bulk of the separator, improving sulfur utilization. rGO-PI/PSSQ show slightly better discharge capacities than rGO-Celgard at 0.1 and 0.2C, following the trend that their respective pristine separators display. However, at 2C cycling rGO-PI/PSSQ yields a far higher discharge capacity (537 mAh/g) than that of rGO-Celgard (204 mAh/g) because non-woven PI/PSSQ separators are superior than Celgard for high-rate cycling performance. The additional rGO interlayer does however lower discharge capacity at 2C for PI/PSSQ compared to the pristine case. This can be attributed to the added layer acting as a physical barrier for lithium ions at higher rates, reducing ion transport and hindering reaction kinetics to some extent. Interlayer loading and electrolyte ratio could be further optimized to eliminate this drop in capacity at 2C for rGO-PI/PSSQ separators. After returning to 0.1 C charge/discharge rates, both rGO-coated separators displayed better capacity than the pristine separators, indicating better entrapment of polysulfide species in the cathode region due to the interlayers. rGO-PI/PSSQ was able to recover to 1010 mAh/g, whereas rGO-Celgard recovered to 960 mAh/g, maintaining the better performance over Celgard observed at the initial 0.1C cycling.

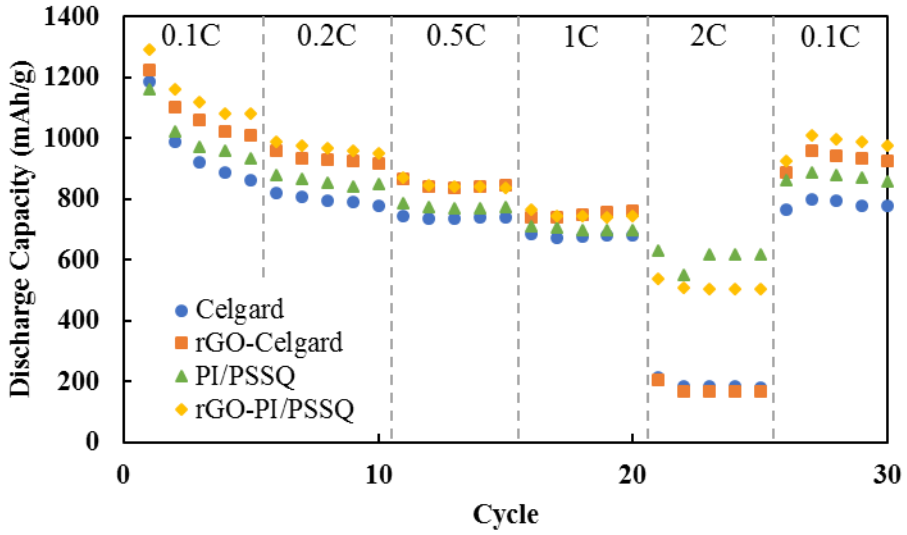


**Figure 3.4.** Performance of Li-S cells with coated and uncoated separators at different charge/discharge current densities.

## 3.4 Conclusion

Previously developed non-woven polyimide/polysilsesquioxane hybrid separators can serve as a framework for further separator modifications to improve lithium-sulfur battery performance, especially at high rates. rGO was applied as an interlayer to these PI/PSSQ separators using a facile air-controlled electrospraying technique. Deposited rGO layers were more loosely structured on the non-woven membranes than microporous Celgard due to differences in their surface roughness. The added coating improved ionic conductivity for both separators, while increasing electrolyte uptake for Celgard and decreasing it for PI/PSSQ. These rGO interlayers improved electrical conductivity at the cathode/separator interface, serving as a secondary current collector to enhance rate performance up to 1C for both Celgard and PI/PSSQ

separators. However, rGO-PI/PSSQ shows far superior 2C cyclability compared to rGO-Celgard due to the improved base separator employed.

## References


(1) Tarascon, J. M.; Armand, M. Issues and Challenges Facing Rechargeable Lithium Batteries. *Nature* **2001**, *414* (6861), 359–367. https://doi.org/10.1038/35104644.

(2) Scrosati, B.; Garche, J. Lithium Batteries: Status, Prospects and Future. *Journal of Power Sources*. 2010, pp 2419–2430. https://doi.org/10.1016/j.jpowsour.2009.11.048.

(3) Larcher, D.; Tarascon, J. M. Towards Greener and More Sustainable Batteries for Electrical Energy Storage. *Nature Chemistry*. 2015, pp 19–29. https://doi.org/10.1038/nchem.2085.

(4) Bruce, P. G.; Freunberger, S. A.; Hardwick, L. J.; Tarascon, J. M. Li-O2 and Li-S Batteries with High Energy Storage. *Nat. Mater.* **2012**, *11* (1), 19–29. https://doi.org/10.1038/nmat3191.

(5) Manthiram, A.; Fu, Y.; Su, Y. S. Challenges and Prospects of Lithium-Sulfur Batteries. *Acc. Chem. Res.* **2013**, *46* (5), 1125–1134. https://doi.org/10.1021/ar300179v.

(6) Ellis, B. L.; Lee, K. T.; Nazar, L. F. Positive Electrode Materials for Li-Ion and Li-Batteries. *Chem. Mater.* **2010**, *22* (3), 691–714. https://doi.org/10.1021/cm902696j.

(7) Fan, X.; Sun, W.; Meng, F.; Xing, A.; Liu, J. Advanced Chemical Strategies for Lithium–Sulfur Batteries: A Review. *Green Energy and Environment*. Elsevier Ltd 2018, pp 2–19. https://doi.org/10.1016/j.gee.2017.08.002.

(8) Yin, Y. X.; Xin, S.; Guo, Y. G.; Wan, L. J. Lithium-Sulfur Batteries: Electrochemistry, Materials, and Prospects. *Angewandte Chemie - International Edition*. 2013, pp 13186–13200. https://doi.org/10.1002/anie.201304762.

(9) Ji, X.; Lee, K. T.; Nazar, L. F. A Highly Ordered Nanostructured Carbon-Sulphur Cathode for Lithium-Sulphur Batteries. *Nat. Mater.* **2009**, *8* (6), 500–506. https://doi.org/10.1038/nmat2460.

(10) Dörfler, S.; Hagen, M.; Althues, H.; Tübke, J.; Kaskel, S.; Hoffmann, M. J. High Capacity Vertical Aligned Carbon Nanotube/Sulfur Composite Cathodes for Lithium-Sulfur Batteries. *Chem. Commun.* **2012**, *48* (34), 4097–4099. https://doi.org/10.1039/c2cc17925c.

(11) Guo, J.; Xu, Y.; Wang, C. Sulfur-Impregnated Disordered Carbon Nanotubes Cathode for Lithium-Sulfur Batteries. *Nano Lett.* **2011**, *11* (10), 4288–4294. https://doi.org/10.1021/nl202297p.

(12) Cheng, X. B.; Huang, J. Q.; Zhang, Q.; Peng, H. J.; Zhao, M. Q.; Wei, F. Aligned Carbon Nanotube/Sulfur Composite Cathodes with High Sulfur Content for Lithium-Sulfur Batteries. *Nano Energy* **2014**, *4*, 65–72. https://doi.org/10.1016/j.nanoen.2013.12.013.

(13) Ji, L.; Rao, M.; Zheng, H.; Zhang, L.; Li, Y.; Duan, W.; Guo, J.; Cairns, E. J.; Zhang, Y. Graphene Oxide as a Sulfur Immobilizer in High Performance Lithium/Sulfur Cells. *J. Am. Chem. Soc.* **2011**, *133* (46), 18522–18525. https://doi.org/10.1021/ja206955k.

(14) Zhang, L.; Ji, L.; Glans, P. A.; Zhang, Y.; Zhu, J.; Guo, J. Electronic Structure and Chemical Bonding of a Graphene Oxide-Sulfur Nanocomposite for Use in

Superior Performance Lithium-Sulfur Cells. *Phys. Chem. Chem. Phys.* **2012**, *14* (39), 13670–13675. https://doi.org/10.1039/c2cp42866k.

(15) Wang, H.; Yang, Y.; Liang, Y.; Robinson, J. T.; Li, Y.; Jackson, A.; Cui, Y.; Dai, H. Graphene-Wrapped Sulfur Particles as a Rechargeable Lithium-Sulfur Battery Cathode Material with High Capacity and Cycling Stability. *Nano Lett.* **2011**, *11* (7), 2644–2647. https://doi.org/10.1021/nl200658a.

(16) Chen, K.; Cao, J.; Lu, Q.; Wang, Q.; Yao, M.; Han, M.; Niu, Z.; Chen, J. Sulfur Nanoparticles Encapsulated in Reduced Graphene Oxide Nanotubes for Flexible Lithium-Sulfur Batteries. *Nano Res.* **2018**, *11* (3), 1345–1357. https://doi.org/10.1007/s12274-017-1749-2.

(17) Oh, C.; Yoon, N.; Choi, J.; Choi, Y.; Ahn, S.; Lee, J. K. Enhanced Li-S Battery Performance Based on Solution-Impregnation-Assisted Sulfur/Mesoporous Carbon Cathodes and a Carbon-Coated Separator. *J. Mater. Chem. A* **2017**, *5* (12), 5750–5760. https://doi.org/10.1039/c7ta01161j.

(18) Zheng, G.; Yang, Y.; Cha, J. J.; Hong, S. S.; Cui, Y. Hollow Carbon Nanofiber-Encapsulated Sulfur Cathodes for High Specific Capacity Rechargeable Lithium Batteries. *Nano Lett.* **2011**, *11* (10), 4462–4467. https://doi.org/10.1021/nl2027684.

(19) Zhang, X. Q.; He, B.; Li, W. C.; Lu, A. H. Hollow Carbon Nanofibers with Dynamic Adjustable Pore Sizes and Closed Ends as Hosts for High-Rate Lithium-Sulfur Battery Cathodes. *Nano Res.* **2018**, *11* (3), 1238–1246. https://doi.org/10.1007/s12274-017-1737-6.

(20) Su, Y. S.; Manthiram, A. Lithium-Sulphur Batteries with a Microporous Carbon Paper as a Bifunctional Interlayer. *Nat. Commun.* **2012**, *3*, 1166. https://doi.org/10.1038/ncomms2163.

(21) Deng, N.; Kang, W.; Liu, Y.; Ju, J.; Wu, D.; Li, L.; Hassan, B. S.; Cheng, B. A Review on Separators for Lithium-Sulfur Battery: Progress and Prospects. *J. Power Sources* **2016**, *331*, 132–155. https://doi.org/10.1016/j.jpowsour.2016.09.044.

(22) Su, Y. S.; Manthiram, A. A New Approach to Improve Cycle Performance of Rechargeable Lithium-Sulfur Batteries by Inserting a Free-Standing MWCNT Interlayer. *Chem. Commun.* **2012**, *48* (70), 8817–8819. https://doi.org/10.1039/c2cc33945e.

(23) Lee, J.; Ko, B.; Kang, J.; Chung, Y.; Kim, Y.; Halim, W.; Lee, J. H.; Joo, Y. L. Facile and Scalable Fabrication of Highly Loaded Sulfur Cathodes and Lithium–Sulfur Pouch Cells via Air-Controlled Electrospray. *Mater. Today Energy* **2017**, *6*, 255–263. https://doi.org/10.1016/j.mtener.2017.11.003.

(24) Li, F.; Zhou, G.; Pei, S.; Li, L.; Wang, D. W.; Wang, S.; Huang, K.; Yin, L. C.; Cheng, H. M. A Graphene-Pure-Sulfur Sandwich Structure for Ultrafast, Long-Life Lithium-Sulfur Batteries. *Adv. Mater.* **2014**, *26* (4), 625–631. https://doi.org/10.1002/adma.201302877.

(25) Du, Z.; Guo, C.; Wang, L.; Hu, A.; Jin, S.; Zhang, T.; Jin, H.; Qi, Z.; Xin, S.; Kong, X.; et al. Atom-Thick Interlayer Made of CVD-Grown Graphene Film on Separator for Advanced Lithium-Sulfur Batteries. *ACS Appl. Mater. Interfaces* **2017**, *9* (50), 43696–43703. https://doi.org/10.1021/acsami.7b14195.

(26) Yao, H.; Yan, K.; Li, W.; Zheng, G.; Kong, D.; Seh, Z. W.; Narasimhan, V. K.; Liang, Z.; Cui, Y. Improved Lithium-Sulfur Batteries with a Conductive Coating on the Separator to Prevent the Accumulation of Inactive S-Related Species at the Cathode-Separator Interface. *Energy Environ. Sci.* **2014**, *7* (10), 3381–3390. https://doi.org/10.1039/c4ee01377h.

(27) Fan, C. Y.; Yuan, H. Y.; Li, H. H.; Wang, H. F.; Li, W. L.; Sun, H. Z.; Wu, X. L.; Zhang, J. P. The Effective Design of a Polysulfide-Trapped Separator at the Molecular Level for High Energy Density Li-S Batteries. *ACS Appl. Mater. Interfaces* **2016**, *8* (25), 16108–16115. https://doi.org/10.1021/acsami.6b04578.

(28) Lu, Y.; Gu, S.; Guo, J.; Rui, K.; Chen, C.; Zhang, S.; Jin, J.; Yang, J.; Wen, Z. Sulfonic Groups Originated Dual-Functional Interlayer for High Performance Lithium-Sulfur Battery. *ACS Appl. Mater. Interfaces* **2017**, *9* (17), 14878–14888. https://doi.org/10.1021/acsami.7b02142.

(29) Huang, J. Q.; Zhang, Q.; Peng, H. J.; Liu, X. Y.; Qian, W. Z.; Wei, F. Ionic Shield for Polysulfides towards Highly-Stable Lithium-Sulfur Batteries. *Energy Environ. Sci.* **2014**, *7* (1), 347–353. https://doi.org/10.1039/c3ee42223b.

(30) Bauer, I.; Thieme, S.; Brückner, J.; Althues, H.; Kaskel, S. Reduced Polysulfide Shuttle in Lithium-Sulfur Batteries Using Nafion-Based Separators. *J. Power Sources* **2014**, *251*, 417–422. https://doi.org/10.1016/j.jpowsour.2013.11.090.

(31) Lee, J. H.; Kang, J.; Kim, S. W.; Halim, W.; Frey, M. W.; Joo, Y. L. Effective Suppression of the Polysulfide Shuttle Effect in Lithium-Sulfur Batteries by Implementing RGO-PEDOT:PSS-Coated Separators via Air-Controlled Electrospray. *ACS Omega* **2018**, *3* (12), 16465–16471. https://doi.org/10.1021/acsomega.8b02551.

(32) Halim, W.; Lee, J. H.; Park, S. M.; Zhang, R.; Sarkar, S.; O'Neil, T.; Chiang, Y. C.; Joo, Y. L. Directly Deposited Binder-Free Sulfur Electrode Enabled by Air-Controlled Electrospray Process. *ACS Appl. Energy Mater.* **2019**, *2* (1), 678–686. https://doi.org/10.1021/acsaem.8b01694.

(33) Zhang, Z.; Lai, Y.; Zhang, Z.; Zhang, K.; Li, J. Al2O3-Coated Porous Separator for Enhanced Electrochemical Performance of Lithium Sulfur Batteries. *Electrochim. Acta* **2014**, *129*, 55–61. https://doi.org/10.1016/j.electacta.2014.02.077.

(34) Kolosnitsyn, V. S.; Kuzmina, E. V.; Karaseva, E. V.; Mochalov, S. E. A Study of the Electrochemical Processes in Lithium-Sulphur Cells by Impedance Spectroscopy. *J. Power Sources* **2011**, *196* (3), 1478–1482. https://doi.org/10.1016/j.jpowsour.2010.08.105.

# Chapter 4. Challenges and Future Work

## 4.1 Challenges of Non-Woven Separators in Lithium-Sulfur

Over the course of this thesis work, many challenges needed to be overcome that were not discussed in the previous chapters, and a better understand and potentially better separators can be developed by investigating them further. Two main failure modes were commonly observed when applying polymer/ceramic non-woven separators to lithium-sulfur (Li-S) and will be first discussed. The methods of overcoming these challenges can be categorized into optimizing the electrolyte ratio, separator thickness, and separator diameter.

### 4.1.1 Failure Modes for Polymer/Ceramic Non-Woven Separators in Lithium-Sulfur

The first failure mode was that after making cells with PI or PI/PSSQ separators, the open circuit voltage (OCV) of the cell would sometimes only be between 0.2 to 0.4 V, within an hour after making the cell. Consequently, these cells would show odd behavior when attempting to cycle them. Upon opening these cells, it was observed that the aluminum current collector of the cathode had been corroded, becoming brittle and easily broken into flakes as shown in Fig. 4.1a. This phenomenon was not seen for Celgard separators at the same electrolyte ratio and was attributed to a higher amount of polysulfides being generated after assembly and the higher diffusivity of dissolved species from one electrode to the other through the non-woven separators. This was confirmed by making Li-S cells without any separator (sulfur cathode and lithium in

direct contact, with added electrolyte) that also showed the aluminum corrosion, since the polysulfides could freely be generated and shuttle between the electrodes. Aluminum corrosion does not seem to be directly caused by the presence of polysulfides, as soaking aluminum or a slurry cathode directly in a 4 mM $Li_2S_6$ in 1:1 DOL:DME by volume solution did not lead to corrosion, even after several days. Further studies should be completed to understand the corrosion mechanism, as it may be an obstacle for designing thinner non-woven separators in Li-S.

The second was semi-infinite charging in the first charge cycle at low 0.2C rates, as shown in Fig. 4.1b. In the cells that did not show low OCV, this other problem was persistent. Dissolved lithium polysulfides potentially have faster diffusion through the highly porous non-woven separators than the narrow slit-like pores of Celgard. This fast shuttling between electrodes could lead to an "infinite charge" where the cell voltage cannot reach the upper cutoff due to continuous oxidation of polysulfide species.

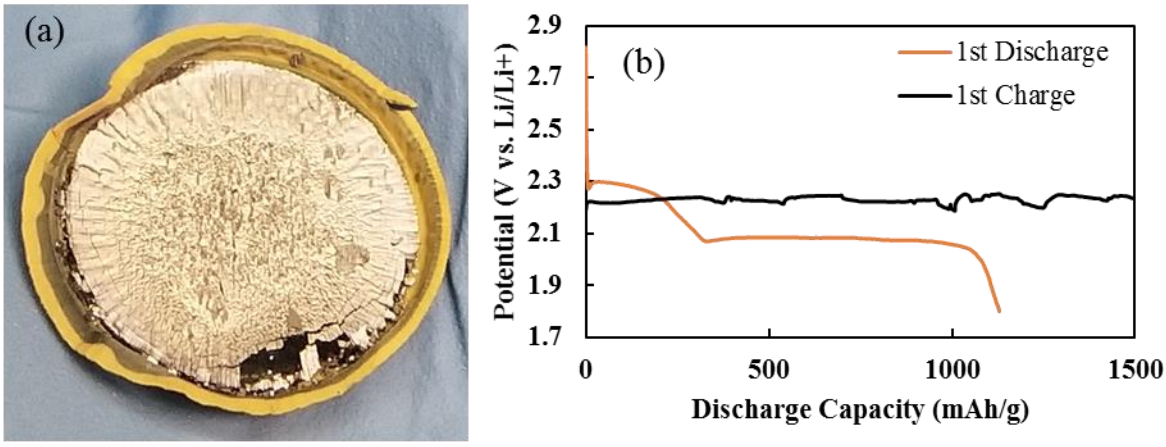


**Figure 4.1.** (a) Digital photograph of corroded aluminum foil current collector, and (b) example of 1st cycle infinite charge with 90/10 PI/PSSQ separator.

### 4.1.2 Optimal Electrolyte Ratio

In lithium-sulfur research the electrolyte is typically added in a specific ratio of electrolyte to active sulfur amount (e.g. μL electrolyte per mg sulfur). The optimal electrolyte ratio depends on the cathode and separator types, as well as the cell configuration employed. Too much electrolyte may cause more rapid capacity fade due to an enhanced polysulfide shuttle effect. On the other hand, too little may lead to premature cell failure from electrolyte degradation as the battery cycles, or higher overpotential and lower overall capacity from the cell components not being properly wetted. When an electrolyte ratio was first employed, a high 40 μL/mg S was used, which exacerbated the failure modes for non-woven separators discussed previously. Reducing this ratio helped to minimize the occurrence of these types of failure but did not eliminate them completely.

In Chapters 2 and 3 of this thesis, a ratio of 15 μL/mg S was used for both uncoated microporous polyolefin and non-woven composite separators. This ratio was optimized for the traditional separator only, so that there was a fairer comparison between the separator types by using the same ratio and not diminishing battery performance for the reference to enhance the benefits of the non-woven separators. The higher electrolyte uptake and enhanced ionic conductivity of PI/PSSQ potentially allows an even lower electrolyte ratio to be used, which should be explored further. The battery cycling results for PI/PSSQ separators could be further improved with an electrolyte ratio optimized for them.

### 4.1.3 Separator Diameter

To circumnavigate the problem of aluminum corrosion, sulfur cathodes deposited onto stainless steel spacers were used to get more reliable battery data and optimize the separators further. The details of these cathodes are not important for this discussion, and it was shown that they gave similar performance to typical cathodes deposited onto aluminum. First cycle infinite charging was still observed for some cells, but overall they were able to cycle reliably. It was found that Li-S cells with PI/PSSQ showed faster capacity fading than commercial Celgard, as shown in Fig. 4.2a. Changing the electrolyte ratio and separator density had little effect on this faster fading behavior.

However, using a PI/PSSQ separator with a smaller diameter of 16 mm rather than 19 mm reduced the capacity fade to that of cells with Celgard, as shown in Fig. 4.2b. The non-woven nature of the PI/PSSQ membranes allows lateral diffusion of polysulfides through the separator. Since the sulfur cathodes employed in this work had a diameter of 15 mm, and the inner diameter of the smaller CR2032 coin cell cap is 16 mm, 19 mm separators contains a lot of excess material that can be pushed to electrochemically inactive regions within the coin cell. For the slit-like pores of Celgard there is minimal lateral diffusion, so polysulfides will not diffuse to the inactive regions of the cell by means of the separator, causing both 16 mm and 19 mm Celgard separators to yield similar capacity fading behavior. Reducing the diameter of PI and PI/PSSQ separators minimizes the inactive regions that polysulfides can diffuse into, limiting the capacity fade seen.

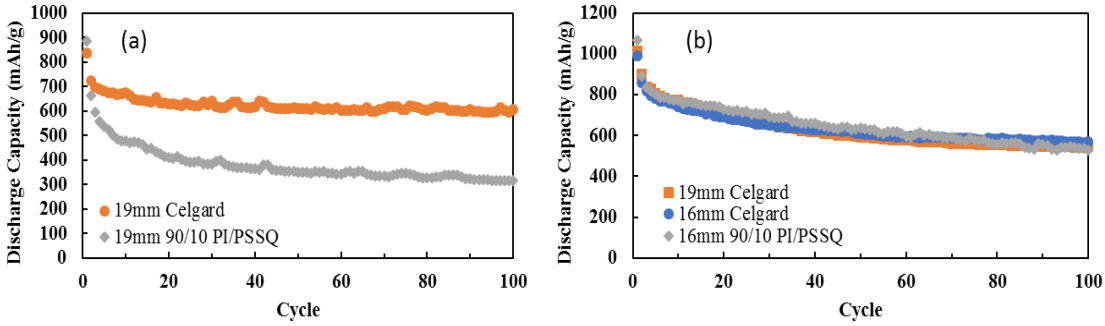


**Figure 4.2.** (a) 0.2C cycling of 19 mm Celgard and 90/10 PI/PSSQ separators, and (b) 0.2C cycling comparison of 16 mm to 19 mm separators

### 4.1.4 Separator Thickness

The non-woven separators initially being used were calendered to 25 µm, which is the thickness of the reference Celgard used and benchmark for lithium-ion batteries. After sorting out the electrolyte ratio and separator diameter and moving back to aluminum-based slurry cathodes for better overall performance, the two main failure mechanisms were still present. It was thought that by providing a larger barrier between the two electrodes, there would be greater resistance to polysulfide diffusion, thus minimizing the failure mechanisms. By using separators with areal loadings of about 2 mg/cm$^2$ and higher, and cold-calendering them to 50 µm, these types of failure were eliminated. As discussed in Chapter 2, these separators are still believed to be the thinnest non-woven separators for Li-S.

## 4.2 Polyimide/Ceramic Separators as a Framework for Further Separator Modifications

The polyimide/polysilsesquioxane separators developed in Chapter 2 can serve as an improved foundation for the typical separator or electrolyte modifications found in lithium-sulfur literature. The reduce graphene oxide (rGO) interlayer investigated in Chapter 3 shows the efficacy of one such modification. However, rGO only provides a physical barrier to stop polysulfides from shuttling to the anode. Developing interlayers that can physically or chemically trap polysulfides in the cathode region as well could further enhance the obtained battery performance. Initial work on a few such interlayers has been completed, but they need to be developed further. Another interesting Li-S modification is the use of gelled electrolyte.

### 4.2.1 Various Interlayers Applied to Polyimide/Ceramic Separators

Many different types of interlayers have been developed for Li-S systems, but most have been applied to basic microporous membranes. The rGO interlayer for PI/PSSQ separators developed in Chapter 3 provided an upper current collector to reduce dissolved polysulfides and improve sulfur utilization even at low current densities. Various other interlayers have been attempted, on either PI/PSSQ or Celgard membranes, but the electrolyte ratio needs to be adjusted for the different coatings to obtain optimal Li-S performance. All interlayers were applied using the air-controlled electrospray method.

One potential interlayer is to coat the surface of PI/PSSQ separators with a polymer, such as PVDF-HFP, to provide a more solid additional layer to prevent

bulky polysulfides from shuttling through the separator. A polymer coating is more densely packed than rGO sheets and offers greater resistance to polysulfide diffusion. One such coating is shown in Fig. 4.3. At the loading applied, the PVDF-HFP coating reveals areas of total (Fig. 4.3a) and partial (Fig. 4.3b) coverage on the non-woven membrane. It is not clear which would be more beneficial to block polysulfide diffusion while not impeding lithium ion transport and overall cell performance.

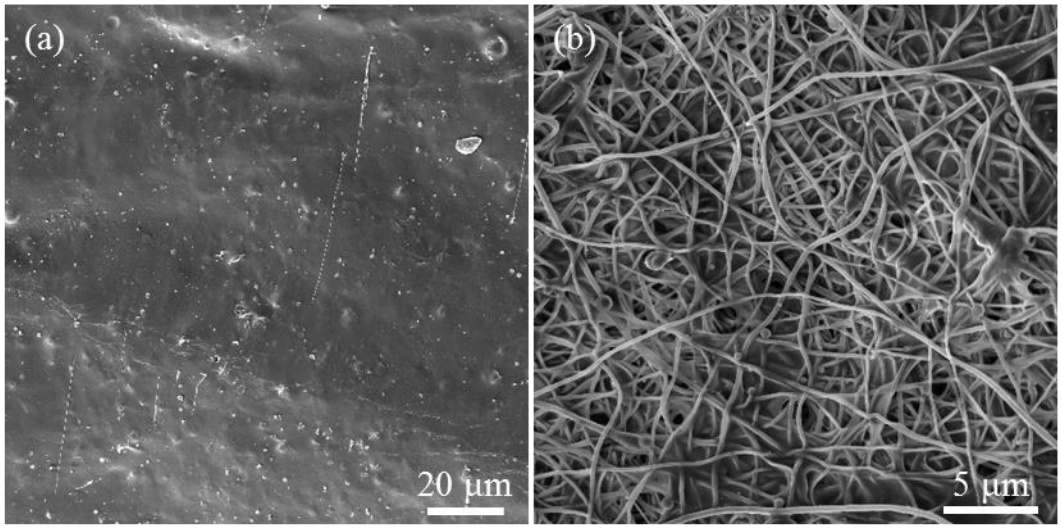


**Figure 4.3.** 90/10 PI/PSSQ separator coated with 0.48 mg/cm$^2$ PVDF-HFP, revealing (a) completely coated and (b) partially coated regions.

Another interlayer that has been initially explored on PI/PSSQ was an additional PSSQ coating. This layer is shown in Fig. 4.4, where it helps to bind fibers together and fill some of the surface pore space of the non-woven membrane, similarly to PVDF-HFP in Fig. 4.3b. A ceramic interlayer has the added benefit of Lewis acid-base interactions with the electrolyte to improve electrolyte affinity of the overall separator, and potentially ionic conductivity.

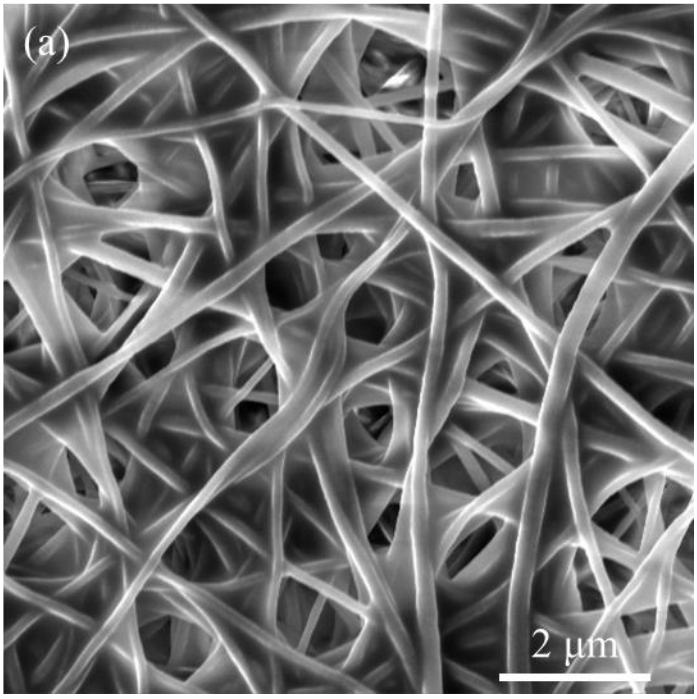


**Figure 4.4.** 90/10 PI/PSSQ separator coated with an initial 0.42 mg/cm$^2$ layer of PSSQ, then heat treated at 300 °C for 3 hours under air.

Several carbon/polymer hybrid interlayers were also coated on Celgard separators. rGO combined with a polyacrylic acid (PAA) binder increases the strength of the layer compared to the roughly stacked rGO sheets shown in Chapter 3 and prevents possible crack formation. Using a more ionically conductive polymer in combination with electrically conductive rGO should allow the interlayer to more easily allow the passage of lithium ions while trapping polysulfides and allowing them to remain electrochemically active through the electrically conductive pathways the rGO provides. To this effect, interlayers of rGO/Nafion and rGO/PEDOT:PSS have also been electrosprayed onto the surface of Celgard. Increased electrolyte needs to be

added to with these layers to ensure proper wetting and reduce the overpotential for reactions to occur.

### 4.2.2 Pre-Gelled Polyimide/Ceramic Separators for Lithium-Sulfur Batteries

A polymer "cage" can be formed around liquid electrolyte, known as gel polymer electrolyte (GPE). These GPEs are an intermediate between liquid electrolyte and solid electrolytes, as they combine aspects of both. In lithium-sulfur, GPE can help to reduce polysulfide shuttling by lowering their solubility in the electrolyte, suppress dendrite formation, and improve overall battery safety.[1] However, GPEs tend to suffer from reduced ionic conductivity and poor performance at higher charge/discharge rates.[1] One method to form GPEs is by adding a reactive monomer and an initiator to liquid electrolyte, then applying ultraviolet irradiation or heat to crosslink the monomers.[2,3] Synthesizing the GPE in this manner lowers interfacial resistance with the electrodes.

Higher ionic conductivity of non-woven PI/PSSQ separators could help to balance the obstruction caused by gelling electrolyte. The PI/PSSQ separators showed improved performance at high rates compared to Celgard, so combining these with GPE could show superior high-rate performance against gelled Celgard as well. Using GPE with PI/PSSQ separators also has the added safety benefits from reducing liquid electrolyte leakage and potentially limiting dendrite penetration. However, the high electrolyte uptake of PI/PSSQ may cause a high uptake of polysulfides before the liquid electrolyte is gelled, trapping a significant portion of polysulfides in the

separator. Therefore, a method of pre-gelling the separator before assembling it in a Li-S cell should be explored and compared to the traditional method.

## 4.3 Use of Alternative Polyimides and Ceramics for Lithium-Sulfur Non-Woven Separators

There are various other combinations of polyimide and ceramics that could be explored for electrospun polyimide/ceramic separators. In Chapters 2 and 3, a soluble version of polyimide (P84, Evonik) was used. However, other forms of soluble polyimide exist with different chemical structures, which may enhance electrolyte interactions and affect membrane properties such as fiber size and swelling in liquid. One such polyimide has the structure termed Matrimid, and is commercially available.[4] The most studied route to forming electrospun polyimides is through electrospinning the soluble polyimide precursor, known as polyamic acid.[5,6] After electrospinning, the obtained fiber mats go through a series of heat treatment steps to imidize the precursor, resulting in polyimide fibers.

Other routes to forming electrospun polymer/ceramic composite electrospun fibers include adding ceramic particles directly into the solution to be spun,[6,7] or adding ceramic precursors instead to avoid issues such as particle aggregation and phase separation.[8–10] Organopolysilazane (OPSZ) is a liquid silicon oxycarbide precursor that is readily miscible with polyimide/N,N-Dimethylformamide (DMF) solutions, and can form ceramic domains within and on the surface of fibers.[9]

In Chapters 2 and 3, P84 polyimide was used with a ladder polysilsesquioxane known as PMK (DJ Semichem). Electrospun fiber mats were also made with Matrimid/PMK

and Matrimid/OPSZ (EMD Performance Materials) combinations, using similar electrospinning conditions as for P84/PMK that could be further optimized. For Matrimid combinations, the initial polymer concentration was set at 17.5 wt% in DMF. Up 30 wt% solid content of ceramic in the fibers was attempted for both P84 and PMK in Matrimid. Issues with either large (approaching 1 μm) fibers or bead formation were present at high ceramic concentrations but altering the conditions could solve these problems. Examples of 90/10 Matrimid/PMK and Matrimid/OPSZ are shown in Fig. 4.5. Using OPSZ improved the ease of spinning, but time sensitivity issues were observed because the OPSZ precursor can begin to cure at room temperature while electrospinning is ongoing. Different polyimides and ceramic combinations should be investigated for use as separators in lithium-sulfur batteries.

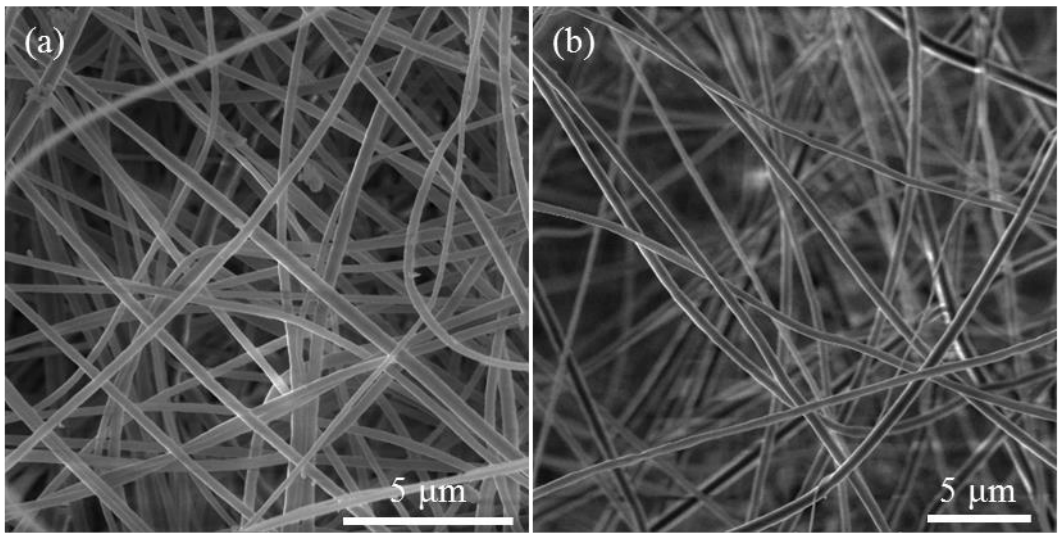


**Figure 4.5.** Digital images of (a) 90/10 Matrimid/PSSQ and (b) 90/10 Matrimid/OPSZ.

## References


(1) Xu, K. Electrolytes and Interphases in Li-Ion Batteries and Beyond. *Chem. Rev.* **2014**, *114* (23), 11503–11618. https://doi.org/10.1021/cr500003w.

(2) Liu, M.; Zhou, D.; He, Y. B.; Fu, Y.; Qin, X.; Miao, C.; Du, H.; Li, B.; Yang, Q. H.; Lin, Z.; et al. Novel Gel Polymer Electrolyte for High-Performance Lithium-Sulfur Batteries. *Nano Energy* **2016**, *22*, 278–289. https://doi.org/10.1016/j.nanoen.2016.02.008.

(3) Zhou, D.; He, Y. B.; Cai, Q.; Qin, X.; Li, B.; Du, H.; Yang, Q. H.; Kang, F. Investigation of Cyano Resin-Based Gel Polymer Electrolyte: In Situ Gelation Mechanism and Electrode-Electrolyte Interfacial Fabrication in Lithium-Ion Battery. *J. Mater. Chem. A* **2014**, *2* (47), 20059–20066. https://doi.org/10.1039/c4ta04504a.

(4) Comer, A. C.; Kalika, D. S.; Rowe, B. W.; Freeman, B. D.; Paul, D. R. Dynamic Relaxation Characteristics of Matrimid® Polyimide. *Polymer (Guildf).* **2009**, *50* (3), 891–897. https://doi.org/10.1016/j.polymer.2008.12.013.

(5) Miao, Y. E.; Zhu, G. N.; Hou, H.; Xia, Y. Y.; Liu, T. Electrospun Polyimide Nanofiber-Based Nonwoven Separators for Lithium-Ion Batteries. *J. Power Sources* **2013**, *226* (February 2014), 82–86. https://doi.org/10.1016/j.jpowsour.2012.10.027.

(6) Shayapat, J.; Chung, O. H.; Park, J. S. Electrospun Polyimide-Composite Separator for Lithium-Ion Batteries. *Electrochim. Acta* **2015**, *170*, 110–121. https://doi.org/10.1016/j.electacta.2015.04.142.

(7) Wang, Y.; Wang, S.; Fang, J.; Ding, L. X.; Wang, H. A Nano-Silica Modified Polyimide Nanofiber Separator with Enhanced Thermal and Wetting Properties for High Safety Lithium-Ion Batteries. *J. Memb. Sci.* **2017**, *537* (January), 248–254. https://doi.org/10.1016/j.memsci.2017.05.023.

(8) Raghavan, P.; Choi, J. W.; Ahn, J. H.; Cheruvally, G.; Chauhan, G. S.; Ahn, H. J.; Nah, C. Novel Electrospun Poly(Vinylidene Fluoride-Co-Hexafluoropropylene)-in Situ SiO2 Composite Membrane-Based Polymer Electrolyte for Lithium Batteries. In *Journal of Power Sources*; 2008; Vol. 184, pp 437–443. https://doi.org/10.1016/j.jpowsour.2008.03.027.

(9) Smith, S. A.; Park, J. H.; Williams, B. P.; Joo, Y. L. Polymer/Ceramic Co-Continuous Nanofiber Membranes via Room-Curable Organopolysilazane for Improved Lithium-Ion Battery Performance. *J. Mater. Sci.* **2017**, *52* (7), 3657–3669. https://doi.org/10.1007/s10853-016-0574-4.

(10) Yanilmaz, M.; Lu, Y.; Zhu, J.; Zhang, X. Silica/Polyacrylonitrile Hybrid Nanofiber Membrane Separators via Sol-Gel and Electrospinning Techniques for Lithium-Ion Batteries. *J. Power Sources* **2016**, *313*, 205–212. https://doi.org/10.1016/j.jpowsour.2016.02.089.